Conformational Distortions of Metalloporphyrins with Electron-Withdrawing NO_2 Substituents at Different Meso Positions. A Structural Analysis by Polarized Resonance Raman Dispersion Spectroscopy and Molecular Mechanics Calculations

Reinhard Schweitzer-Stenner,*,† Christina Lemke,‡ Raid Haddad,§,|| Yan Qiu,§,|| John A. Shelnutt,§,|| J. Martin E. Quirke,⊥ and Wolfgang Dreybrodt‡

Department of Chemistry, University of Puerto Rico, Río Piedras Campus, P.O. Box 23346, San Juan, Puerto Rico 00931, FB1-Institut für Experimentelle Physik, Universität Bremen, 28359 Bremen, Germany, Biomolecular Materials and Interfaces Department, Sandia National Laboratories, Albuquerque, New Mexico 87185-1349, Department of Chemistry, University of New Mexico, Albuquerque, New Mexico 87131 and Department of Chemistry, Florida International University, Miami, Florida 33199

Received: March 12, 2001; In Final Form: March 21, 2001

The meso substituted Ni(II)(5,15-diNO_2−octaethylporphyrin) coexists in at least three different conformers in CS_2. To explore the structural properties of these conformers, we measured the resonance excitation profiles and depolarization ratio dispersions of various prominent Raman lines of Ni(5,15-diNO_2−octaethylporphyrin) in CS_2. The data were analyzed by a theoretical approach, which formulates the Raman tensor in terms of vibronic coupling parameters that depend on static deformations along the normal coordinates. The coupling parameters were determined by simultaneously fitting the depolarization ratio dispersion data and the corresponding resonance excitation profiles. We have also performed molecular mechanics calculations to identify all possible stable conformers of the molecule. To quantify the out-of-plane distortions of the calculated structures, we subjected them to normal coordinate deformation analysis (Jentzen, W.; Song, X.-Z.; Shelnutt, J. A. *J. Phys. Chem. B* **1997**, *101*, 1684). The results obtained from the Raman data and from molecular modeling are consistent in showing that the most stable conformers are strongly affected by rhombic in-plane (0.3 Å) and ruffling (2.1 Å) and doming (0.5−0.6 Å) out-of-plane distortions. Additionally, smaller contributions from saddling were also obtained (∼0.1 Å). The three conformers detectable from the analysis of the Raman spectra most likely differ in terms of saddling and doming. The lowest-energy calculated conformers all show a horizontal orientation and out-of-plane position of the NO_2 groups with respect to the macrocycle, but the conformers differ in the orientations of the ethyl substituents. Conformers with vertical orientations of the NO_2 groups are calculated to be slightly higher in energy. INDO/s calculations reveal that the horizontal NO_2 group orientation, and to a lesser extent the vertical orientation, gives rise to a strong admixture between porphyrin and NO_2 molecular orbitals, enhancing the above distortions and leading to a break down of the 4-orbital model. A comparison with monosubstituted Ni(II)(5-NO_2−OEP) reveals that all distortions increase with increasing number of nitro substituents. Altogether, this study demonstrates that meso nitro substitution of metalloporphyrins has a significant impact on electronic as well as structural properties of the ground and excited electronic states.

Introduction

The structural properties of metalloporphyrins have become a major subject of research over the last 10 years.[1] This particularly concerns the issue of how macrocycle distortions determine physicochemical and functional properties.[2−7] This research is of practical relevance because it aids in designing porphyrins as biosensors[8] and optical switches[9] and also has implications for the understanding of chromophore−protein interactions.[10] Strong evidence has been provided in the meantime that distortions may affect the spin delocalization, redox potential, electronic structure, and vibrational dynamics of the macrocycle[11] as well as the affinity and geometry of axial ligand binding.[1,12] In this context, a strong emphasis has been put on nonplanar distortions, which, in solution and crystals, are mostly caused by steric interactions between peripheral substituents,[1] whereas specific heme protein interactions are the predominant cause in proteins.[6,12,13]

While nonplanar distortions have attracted considerable attention, the number of studies dealing with in-plane distortions induced by asymmetrically arranged peripheral substituents and chromophore−protein interactions are rather limited. Jentzen et al. have investigated a series of nonplanar 5,15-meso substituted porphyrins without focusing on the in-plane distortions.[14,15] Senge et al.[16] have addressed this issue in their recent comparative analysis of the crystal structures of various deca- and undecasubstituted porphyrins with meso alkyl and aryl groups. They found that 5,15 substitution gives rise to a rectangular elongated core characterized by different N···N separations parallel to the 5,15 and 10,20 axes. Interestingly,

* Corresponding author. Tel.: 787-764-0000 (ext 2417). Fax: 787-756-8242. E-mail: rstenner_upr_chemistry@gmx.net.
† University of Puerto Rico.
‡ Universität Bremen.
§ Sandia National Laboratories, Albuquerque.
|| University of New Mexico.
⊥ Florida International University.

10.1021/jp010936+ CCC: $20.00
Published on Web 06/16/2001

this distortion is of comparable magnitude for corresponding free-base and Ni(II) porphyrins. In the language of group theory commonly used to characterize D_{4h} porphyrin deformations, this distortion is of B_{2g} symmetry. This study shows that asymmetric peripheral substituents indeed give rise to symmetry lowering in-plane distortions. Given the asymmetrical substitution of biological chromophores, it is certainly of relevance to put a higher emphasis on in-plane distortions and their functional relevance. It would be also of interest to find out whether in-plane distortion may facilitate out-of-plane distortions and vice versa.

Over the last 15 years, we have developed polarized Raman dispersion spectroscopy (PRDS) as a method to obtain asymmetric distortions of porphyrins in solution and in proteins.[17] The method involves the analysis of resonance excitation profiles (REP), which yields detailed information about the differences between the potential surfaces of excited electronic states and the ground state. Moreover, it provides insights into interferences between scattering amplitudes resulting from different mechanisms involved in the coupling between vibrational and electronic motions. This is particularly relevant for porphyrins, where most of the Raman lines gain intensity from both interstate and intrastate vibronic coupling and also from multimode mixing between different vibronic states.[17] REPs of intense Raman lines can be measured for scattered light polarized parallel and perpendicular to the scattering plane. From this, one obtains depolarization ratios, which provide information about the symmetry of the corresponding normal modes. For undistorted (planar) porphyrins exhibiting D_{4h}, D_{2d}, or D_4 symmetry, the depolarization ratio of all Raman lines does not depend on the excitation wavelength. However, symmetry-lowering distortions may admix different symmetries into the Raman tensor, thus causing strong depolarization ratio dispersion (DPD).[17−19]

In this paper we employ PRDS to investigate the distortions of the asymmetrically meso substituted Ni(5,15-diNO_2−octaethylporphyrin) [Ni(5,15-diNO_2−OEP)] in CS_2. In an earlier study, we have shown that nearly all structure-sensitive Raman lines of this substance show strong DPDs indicative of in-plane and out-of-plane distortions.[20] In the preceding paper,[21] we have reported a thorough spectral and normal coordinate analysis of this porphyrin. Therein, we found that three different coexisting conformers can be distinguished spectroscopically. In the present study, we thoroughly analyze the DPDs and REPs of seven prominent Raman active vibrations to determine how these conformers are affected by planar and nonplanar distortions. The study sheds some light on the mechanism by which the nitro substituents perturb the electronic and structural properties of the macrocycle to yield a molecule which can adopt different conformations with only slightly different free energy.

Theoretical Background

A detailed description of the Raman theory employed to fit resonance excitation profiles (REPs) and the depolarization ratio dispersion (DPD) are given in previous papers.[17,22] Here, we confine ourselves to defining the parameters obtained from our fitting procedure.

First-Order Vibronic Coupling and Selection Rules. In general terms, the Raman tensor elements $\alpha_{\rho\sigma}$ (ρ and $\sigma = x, y, z$) are given by the Kramers−Heisenberg−Dirac equation

$$\alpha_{\rho\sigma} = \sum_{\mathrm{l}} \frac{\langle f|\vec{R}_\rho|l\rangle\langle l|\vec{R}_\sigma|\mathrm{i}\rangle}{E_l - E_g - \Omega_{\mathrm{L}} - \mathrm{i}\Gamma_{\mathrm{l}}} \qquad (1)$$

where $|i\rangle$, $|l\rangle$, and $|f\rangle$ denote the initial, intermediate, and final vibronic state of the scattering process, respectively. $\vec{R}_\rho$ and $\vec{R}_\sigma$ are electronic dipole transition operators. $E_l - E_g$ is the energy difference between intermediate and ground state, whereas the excitation energy is denoted as Ω_{L}. Γ_{l} is the Lorentzian half-width of the absorption band associated with the electronic dipole transition $|i\rangle \rightarrow |l\rangle$. Note that all energies are expressed in units of cm^{-1} throughout this paper.

The vibronic wave functions of porphyrins can be described by a third-order nonadiabatic perturbation expansion of a crude Born Oppenheimer basis. The first-order expansion coefficients reflect vibronic coupling between different excited electronic states $|l_0\rangle$ and $|m_0\rangle$, i.e.

$$c_{lm}^{\Gamma_r} = \left\langle l_0 \left| \frac{\partial \hat{H}_{\mathrm{el}0}}{\partial q_r^{\Gamma_r}} \right| \mathrm{m}_0 \right\rangle \langle 1|q_r^{\Gamma_r}|0\rangle \qquad (2)$$

where $q_r^{\Gamma_r}$ denotes the normal coordinate of the Raman vibration under consideration. $\partial\hat{H}_{\mathrm{el}0}/\partial q_r^{\Gamma_r}$ is the vibronic coupling operator, Γ_{r} is the irreducible representation of the Raman vibration, and $\langle 1|\partial q_r^{\Gamma_r}|0\rangle$ is its transition matrix element for the electronic ground state. In the first order, the Raman cross section of a distinct mode is linearly dependent on the square of its matrix elements $c_{lm}^{\Gamma_r}$.

The pure electronic wave functions of the porphyrin electronic states involved in resonance Raman scattering can be expressed in terms of Gouterman's four-orbital model.[23] It is based on the assumption that the symmetry of the porphyrin macrocycle is D_{4h} and yields the 2-fold degenerate excited singlet states $|B_0\rangle = |B_{x0},B_{y0}\rangle$ and $|Q_0\rangle = |Q_{x0},Q_{y0}\rangle$, which can be calculated from the singly excited configurations composed of these four molecular orbitals. Specifically, these states arise from near 50:50 mixing of the excited electronic configurations $|a_{1u}e_g|$ and $|a_{2u}e_g|$. The two HOMOs of a_{1u} and a_{2u} symmetry are thereby considered to accidentally exhibit nearly the same energies. The ground state is a singlet state of A_{1g} symmetry in which a_{1u} and a_{2u} are filled. The electronic transitions $|g\rangle \rightarrow |Q\rangle$ and $|g\rangle \rightarrow |B\rangle$ give the well-known Q and B bands in the porphyrin optical spectrum.

Since $|Q\rangle$ and $|B\rangle$ transform like the irreducible representation E_u of the D_{4h} point group, group theory dictates that $\Gamma_r = \Gamma(\partial\hat{H}_{\mathrm{el}0}/\partial q_r^{\Gamma_r}) = \Gamma(q_r^{\Gamma_r}) = A_{1g}$, B_{1g}, B_{2g}, or A_{2g} for the symmetry of Raman-active vibrations. Experimentally, Raman bands resulting from these vibrations can be distinguished by measuring their depolarization ratio, which is defined as

$$\rho = \frac{I_\perp}{I_{||}} \qquad (3)$$

where $I_{||}$ and $I_\perp$ denote the scattered intensities measured parallel and perpendicular to the polarization of the exciting laser beam. In solution, the values for the above symmetries are 0.125 for A_{1g}, 0.75 for B_{1g} and B_{2g}, and infinite for A_{2g}, provided that the incident polarization is oriented perpendicular to the scattering plane.

Asymmetric Distortions. Deviations from these depolarization ratio values are indicative of symmetry lowering distortions, which may result from peripheral substituents, axial ligands, and, in proteins, heme−protein contacts. They can be described by

$$\Delta = \sum_\Gamma \Delta^\Gamma = \sum_\Gamma \sum_i \delta\bar{q}_i^{\Gamma_i} \qquad (4)$$

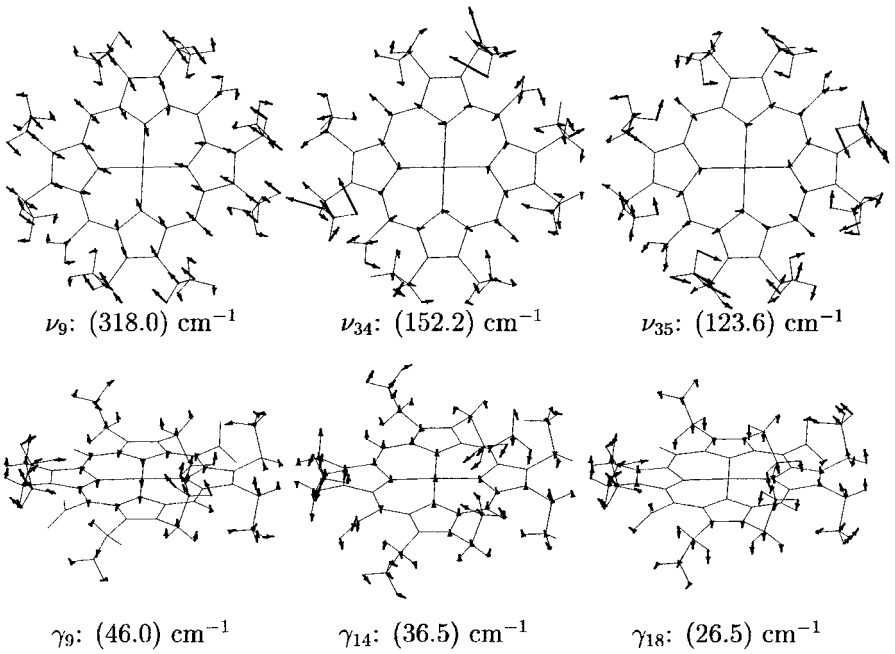

Figure 1. Representations of the SNCDs along the normal coordinates of ν_9(A_{1g}), ν_{34} (B_{2g}), γ_9 (A_{2u}), γ_{14} (B_{1u}), and γ_{18}(B_{2u}).

$\delta\bar{q}_i^{\Gamma_i}$ denotes the amplitudes of the static normal coordinate deformations (SNCD)[15] along the *i*th normal coordinate exhibiting the symmetry Γ_i in D_{4h}. As shown in recent analyses of isolated porphyrins and heme groups, Δ is dominated by distortions along normal coordinates of the lowest wavenumber modes of the respective symmetry representation. In the SNCD analysis, the deformations given are for the normal coordinates of a porphyrin macrocycle with no substituents; when substituents are present, these macrocycle modes become mixed with the substituent modes to give the normal coordinates of the particular substituted porphyrin.

Figure 1 shows graphic representations of five different types of deformations which might affect the structure of Ni(5,15-diNO_2−OEP), namely, a totally symmetric A_{1g} deformation which involves either a contraction or an expansion of the porphyrin core by equivalent displacements of the pyrrole rings or a rhombic distortion of B_{2g} symmetry along the meso carbons which is combined with in-plane distortion of the macrocycle core and saddling (B_{2u}), ruffling (B_{1u}), and doming (A_{2u}) of the macrocycle. These deformations correspond to the normal modes ν_9(A_{1g}), ν_{34} (B_{2g}), γ_{14} (B_{1u}), γ_{18}(B_{2u}), and γ_9(A_{2u}).[21] In-plane B_{1g} and A_{2g} deformations are unlikely because they are inconsistent with the symmetry determined by the peripheral substituents.[23] Out-of-plane propellering (A_{1u}) distortions cannot be ruled out but were found to be unlikely in general because of the energy cost.[15]

Asymmetric distortions give rise to electronic and vibronic perturbations that directly affect the composition of the Raman tensor.[20] They are briefly introduced in the following.

Electronic Perturbations. They can be accounted for by expanding the electronic Hamiltonian $\hat{H}_{el}$ with respect to the above *SNCDs* of the porphyrin's electronic ground state

$$\hat{H}_{el} = \hat{H}_{el_0} + \hat{H}_{\Gamma} \tag{5a}$$

where

$$\hat{H}_{\Gamma} = \sum_j \frac{\partial \hat{H}_{el_0}}{\partial q_j^{\Gamma_j}} \delta\bar{q}_j^{\Gamma_j} \tag{5b}$$

In this study, we only consider totally symmetric contributions to the interaction matrix element, which are written as[17]

$$\delta A_{1g} = \langle Q_{x0}|\hat{H}_{A_{1g}}|B_{x0}\rangle = \langle B_{x0}|\hat{H}_{A_{1g}}|Q_{x0}\rangle \tag{5c}$$

Symmetric perturbations $\delta_{A_{1g}}$ cause an unmixing of Gouterman's 50:50 states in that it separates the accidentally degenerate configurations $|a_{1u}e_g|$ and $|a_{2u}e_g|$.

Though certainly of relevance for Ni(5,10-NO_2−OEP), asymmetric electronic perturbations are not considered explicitly, since, as we will argue below, they cannot be inferred unambiguously from the absorption spectrum.

Vibronic Perturbations. The above SNCDs also affect the vibronic states within a given electronic state and the vibronic coupling properties of the Raman active modes. This can be accounted for by expanding the vibronic coupling operator in eq 2 with respect to $\delta\bar{q}_j^{\Gamma_j}$

$$\frac{\partial \hat{H}_{el}}{\partial q} = \frac{\partial \hat{H}_{el_0}}{\partial q_r^{\Gamma_r}} + \sum_{\Gamma_a}\sum_i \frac{\partial^2 \hat{H}_{el_0}}{\partial q_r^{\Gamma_r}\partial q_i^{\Gamma_i}} \delta\bar{q}_i^{\Gamma_i} + \sum_{\Gamma_a}\sum_j \frac{\partial^3 \hat{H}_{el_0}}{\partial q_r^{\Gamma_r}\partial q_i^{\Gamma_i}\partial q_j^{\Gamma_j}} \delta\bar{q}_i^{\Gamma_i}\delta\bar{q}_j^{\Gamma_j} \tag{6}$$

Term 1 reflects vibronic coupling in an undistorted D_{4h} symmetry. The influence of symmetry lowering distortions is accounted for by the second and third term. To couple states of E_u symmetry, the product representation $\Gamma_r \otimes \Gamma_i$ and $\Gamma_r \otimes \Gamma_i \otimes \Gamma_j$ of the second and third derivatives of the Hamiltonian operators in the second and third term must contain A_{1g}, B_{1g}, B_{2g}, or A_{2g}. As a consequence, in-plane deformations of A_{1g}, B_{1g} B_{2g}, or A_{2g} symmetry contribute via the second-order term, while the third-order term contributes if at least two different out-of-plane deformation of A_{1u}, A_{2u}, B_{1u}, or B_{2u} symmetry exist. Additionally, E_g and E_u deformations may contribute via the third-order term, since the products $E_g \otimes E_g$ and $E_u \otimes E_u$ decompose into $A_{1g} \oplus B_{1g} \oplus B_{2g} \oplus A_{2g}$.

Apparently, the symmetry of a vibronic perturbation is given by the product representations $\Gamma_r \otimes \Gamma_I$ and $\Gamma_r \otimes \Gamma_i \otimes \Gamma_j$ of the

Raman mode $q_r^{\Gamma_r}$ and the SNCDs $\delta\bar{q}_i^{\Gamma_i}$ and $\delta\bar{q}_j^{\Gamma_j}$. It can be obtained from the multiplication Tables S1a and S1b (Supporting Information). In general terms, vibronic perturbations cause an admixture of different symmetries in the Raman tensor. If the macrocycle symmetry is lowered from D_{4h} to C_s, the Raman tensor is written as

$$\hat{\alpha} = \begin{pmatrix} a_{1g}(\Omega_L) + b_{1g}(\Omega_L) & b_{2g}(\Omega_L) + a_{2g}(\Omega_L) \\ b_{2g}(\Omega_L) - a_{2g}(\Omega_L) & a_{1g}(\Omega_L) - b_{1g}(\Omega_L) \end{pmatrix} \quad (7)$$

where the tensor elements $\Gamma(\Omega_L)$ are in first-order written as the weighted sum of respective vibronic coupling matrix elements c_{lm}^{Γ} as defined by eq 2, which now contains a vibronic coupling operator as described by eq 6. The tensor elements depend on the excitation wavenumber Ω_L. Details are given in refs 17 and 22. Since vibronic coupling occurs only between *x* an *y* polarized states, the *z*-components have been disregarded. As a consequence of the symmetry mixing described by eq 7, the depolarization ratio ρ depends now also on Ω_L and can be written in terms of the tensor elements as follows:[20]

$$\rho = \frac{3}{4}\frac{a_{1g}(\Omega_L)^2 + 5a_{2g}(\Omega_L)^2 + 2\lfloor b_{1g}(\Omega_L)^2 + b_{2g}(\Omega_L)^2 \rfloor}{6a_{1g}(\Omega_L)^2 + 2[b_{1g}(\Omega_L)^2 + b_{2g}(\Omega_L)^2]} \quad (8)$$

The matrix coefficients c_{lm}^{Γ} are utilized to express the vibronic wave functions in the Kramers−Heisenberg−Dirac expression of the Raman tensor. The pure electronic wave functions *l* and *m* are identified with Q_x, Q_y, B_x, and B_y of the perturbed electronic system. A complete representation of the Raman tensor is given in earlier publications.[22]

In the Supporting Information, we describe in more detail the relationship between between porphyrin deformations, vibronic perturbations, and the symmetry of the Raman tensor.

Multimode Mixing. The analysis of REPs and DPDs of Raman lines is complicated by the fact that their Raman tensors are not independent. This results from multimode mixing, i.e., the creation and subsequent annihilation of a vibrational quantum of modes different from the observed Raman mode in the scattering process. As a consequence, the vibronic coupling parameters of a distinct Raman mode appear in higher terms of the Raman tensor of all other Raman active vibrations. Hence, it is necessary to perform a simultaneous global fitting to the REPs and DPDs of sufficiently large number of Raman modes. Details are described in references.[17,22]

Inhomogeneous Broadening. The temperature independent inhomogeneous broadening was obtained from absorption spectra taken at low temperatures and was explicitly considered in the final calculation of the Raman cross section. The mathematics is given in ref 22.

Material and Methods

All details about the preparation of the 5-NO_2- and Ni(5,15-diNO_2−OEP), the experimental setup, and the spectral analysis are given elsewhere.[20,21] The strategy adopted to simultaneously fit the DPDs and REPs are also described in an earlier publication.[22] Briefly, the REPs and DPDs obtained from our Raman spectra of Ni(5,15-diNO2−OEP) were fitted by using the vibronic coupling parameters c_{es}^{Γ} appearing in the eqs 9, 11, 13, and 15, and the half-widths Γ of the excited vibronic states were used as free parameters. Moreover, we assumed that the porphyrin vibrations might have different frequencies in the excited states and in the ground state. All fits were carried out by adopting the following iterative procedure:

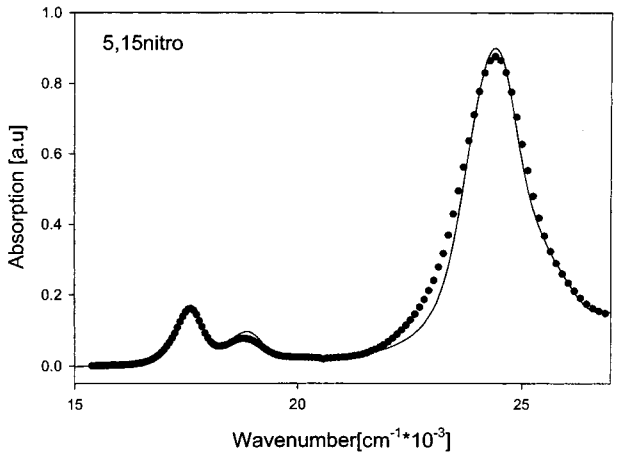

Figure 2. Absorption spectrum of 5,15-NO_2-Ni(II)octaethylporphyrin. The solid lines results from a calculation described in the Results section.

1. In the first step, we estimated the pure electronic resonance energies E^Q and E^B, the corresponding Lorentzian half-widths Γ^Q and Γ^B, the inhomogeneous broadening $\sigma_Q = \sigma_B$ and the ratio $M_{gQ}^{x,y}/M_{gB}^{x,y}$ of the electronic dipole transition moments from the optical spectrum shown in Figure 2. From the latter we determined the electronic parameter $\delta_{A_{1g}}$. We did not try to determine the parameters of electronic perturbations because their direct influence on the optical spectrum and the DPDs can be considered as small for the molecules investigated. They have an indirect influence via the coupling parameters c_{es}^{Γ}.
2. In the second step, these parameters were used in a first fit to the DPDs and REPs of all lines investigated. Multimode mixing was thus neglected.
3. In the third step, we accounted for multimode mixing by inserting the above obtained vibronic coupling parameters of seven Raman active modes into the third-order term of the Raman tensor (see ref 22 for details). The experimental data were now refitted by using only the c_{es}^{Γ} of the considered Raman mode as a variable and the vibronic coupling parameters of the other vibrations as fixed parameters.
4. The last step was repeated until convergence was achieved. It should be emphasized that due to the explicit consideration of multimode mixing the absolute values of the vibronic coupling parameters can be estimated.

As shown below, some of the structure-sensitive Raman lines in the high-frequency region can be decomposed into sublines resulting from different conformers. To appropriately fit their REPs, we have assumed comparable intrinsic intensities for these conformers to estimate their molar concentration. From this, we calculated scaling factors for the theoretically obtained REPs.

Additionally, we have fitted the REPs and DPDs of a few selected Raman lines of Ni(5-diNO_2−OEP). Since the intensities of the vibronic sidebands of the investigated porphyrins are similar, we have used the parameters obtained for Ni(5,15-NO_2−OEP) to simulate the contribution from multimode mixing. Unfortunately, the quality of the data only allows an estimation of the coupling parameters.

Molecular modeling including molecular mechanics and static normal coordinate deformation (SNCD) calculations were carried as described in great detail in earlier publications.[12,15] Different force field parameters (sp2 and sp2 resonance atom types) were tried for the nitrogen and oxygens of the NO_2 group. There were no significant differences in the ordering of the energies of either the vertical and horizontal conformers or the INDO/S results as a result of using different NO_2 parameters.

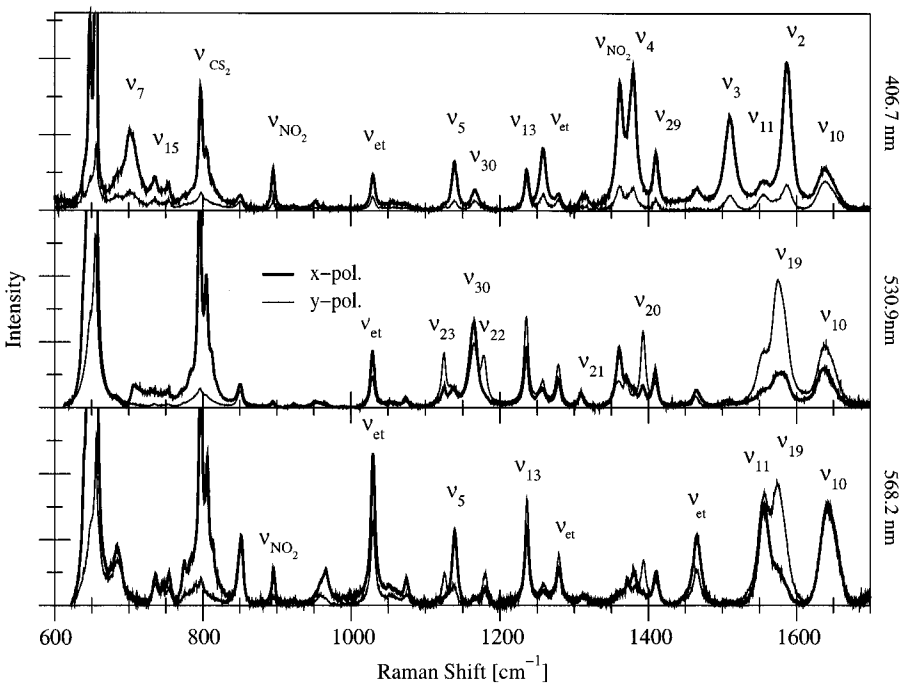

Figure 3. Polarized resonance Raman spectra of Ni(5,15-NO_2−OEP) between 600 and 1800 cm^{-1}, taken at the indicated excitation wavelengths.

Results

Raman Spectra. Figure 3 shows polarized resonance Raman spectra of Ni(5,15-diNO_2−OEP) observed with Soret (406.7 nm), Q_v (530.9 nm) and Q_0 (568.2 nm) excitation between 600 and 1800 cm^{-1}. As expected, the Soret spectrum is dominated by lines from A_{1g}-type modes, while the two Q band spectra mainly feature lines from B_{1g} and A_{2g}-type vibrations. Lines from B_{2g} modes are generally weaker and appear only in the Q_v band spectrum with significant intensities.[24] A total number of 65 spectra taken with different excitation energies were subjected to a global fit as described earlier.[20] The result of this analysis is described and discussed by Lemke et al.[21]

Raman Dispersion Data. We have measured and analyzed the DPDs and REPs of the following Raman lines of 5,15-NO_2-nitro: ν_2 (A_{1g}, ∼1587 cm^{-1}), ν_4 (A_{1g}, 1380 cm^{-1}), ν_{NO_2} (NO_2 symmetric stretch, 1361 cm^{-1}), ν_{10} (B_{1g}, ∼1635 cm^{-1}), ν_{11} (B_{1g}, ∼1554 cm^{-1}), ν_{29} (B_{2g}, 1410 cm^{-1}) and ν_{19} (A_{2g}, ∼1574 cm^{-1}). As discussed in the preceding paper,[21] the Raman lines of ν_2, ν_{11}, and ν_{19} can be decomposed into two sublines with slightly different REPs. For ν_{10}, even three sublines of comparable intensities were obtained.

The DPDs and REPs of the Raman lines investigated are depicted in Figures4−8. The high accuracy of our spectral analysis enabled us to separately determine the DPDs and REPs of all sublines identified. The solid line results from the self-consistent global fit to the data based on the theory described above. In view of the complexity of the data and some limitations of the model (cf. ref 22), the quality of the fits can be judged as very satisfactory. Some systematic deviations between fit and experimental data are only obtained for the DPD of ν_4 (Figure 8) and to a minor extent for ν_{19}, which are discussed below. The electronic and vibronic parameters obtained from the fits are listed in Table 1.

We have used these parameters to calculate the optical absorption spectrum (the relevant equation is given in ref 22). This is always an ultimate test of the validity of the vibronic coupling parameters.[22] If one inserts the full sets of coupling parameters of the Raman lines investigated, one overestimates the vibronic sideband Q_v by a factor of 2. A closer analysis of the different contributions to Q_v revealed, however, that the overestimation is solely caused by the intrastate vibronic coupling parameters $c_{QQ}^{B_{1g}}$ of ν_{10} and ν_{11}, which are much larger than those predicted by the four orbital model (Table 1). They are crucial for a successful fit in particular of the corresponding REPs. In accordance with Unger et al.,[24] we believe that they reflect some vibronic coupling between the d_π orbitals of the metal and the porphyrin ground state interactions which selectively affect the Q band Raman scattering of B_{1g} modes. If one disregards these coupling parameters in the calculation of the absorption spectrum, a very good reproduction of both vibronic sidebands is obtained (solid line in Figure 2). The deviation at the low-energy side of the B band could result from the fact that our calculation did not explicitly take into account the existence of three subbands of different conformers. Altogether, this simulation corroborates the validity of our coupling parameters.

A comparison of the data for $\nu_2(A_{1g})$ and $\nu_{19}(A_{2g})$ (Figures 5 and 6) reveals very similar DPDs. Both lines appear polarized with Soret and inverse polarized with excitations between Q_0 and Q_v. A comparable observation was made earlier for Ni-(OETPP), even though the dispersion of ν_2 is much more pronounced in the present case. The analysis of the data showed that vibronic perturbations of A_{2g} and B_{2g} (vibronic coupling parameters $c_{lm}^{B_{2g}}$ and $c_{QB}^{A_{2g}}$ in Table 1) cause the DPD for $\nu_2(A_{1g})$, while the A_{2g} mode ν_{19} is affected by A_{1g} and B_{1g} perturbations (matrix elements $c_{lm}^{A_{1g}}$ and $c_{lm}^{B_{2g}}$ in Table 1). Table S1b reveals that $c_{QB}^{A_{2g}}(\nu_2)$ and $c_{lm}^{A_{1g}}(\nu_{19})$ result both from saddling (B_{2u}) and ruffling (B_{1u}) distortions, whereas the respective B-type vibronic perturbations $c_{lm}^{B_{2g}}(\nu_2)$ and $c_{lm}^{B_{1g}}(\nu_{19})$ can be due to B_{2g} deformations (Table S1a) and also due to the additional presence of doming (A_{2u}), which, as shown above, causes this type of vibronic perturbation in the presence of ruffling.

The calculated REPs of the two ν_{19} sublines (Figure 5) show some minor deviation from the experimental data. This has two reasons. First, as shown already by Lemke et al.,[20] the vibronic perturbation approach does not fully account for the strong

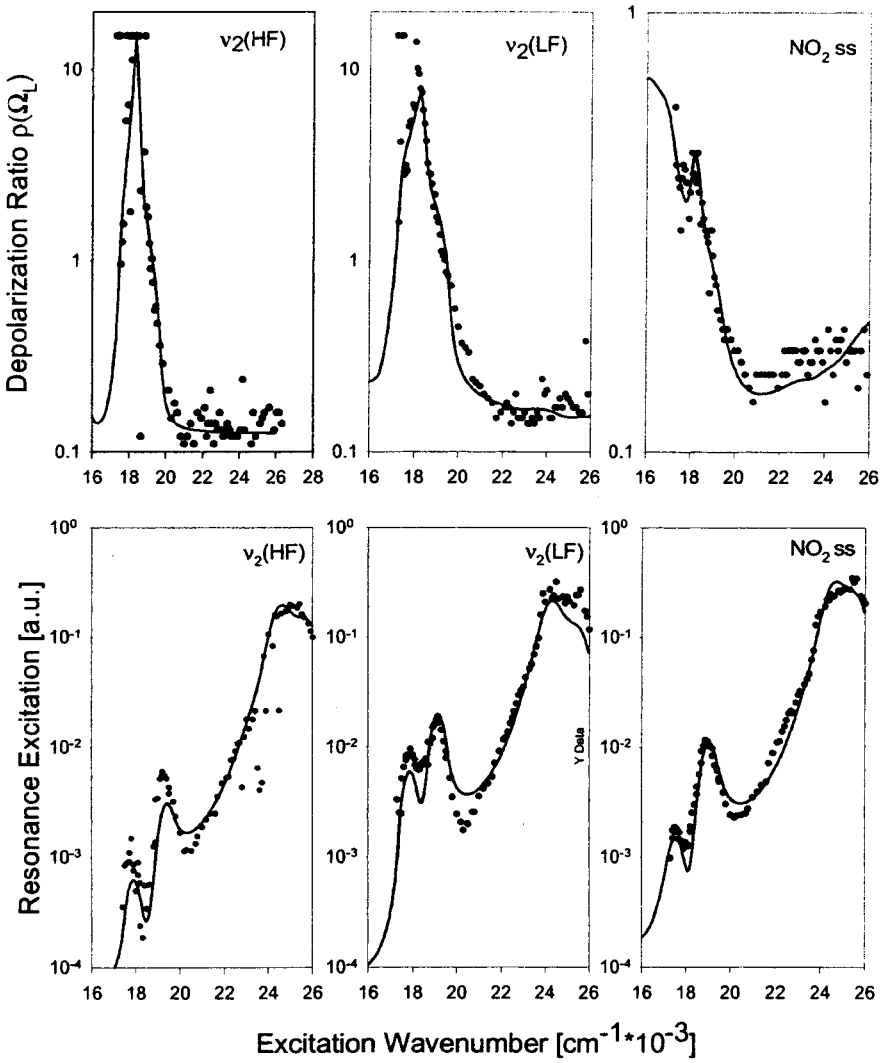

Figure 4. Depolarization dispersion and resonance excitation profiles of the high- and low-frequency subline of A_{1g}-type ν_2 and of the NO_2 symmetric stretching vibration of Ni(5,15-NO_2−OEP). The solid lines result from the fitting procedure outlined in Materials and Methods and Results.

vibronic coupling of ν_{19}. This leads to an underestimation of multimode mixing and thus to an overestimation of the Q_ν/Q_0 intensity ratio. Second, the deviations in the B_ν band region may result from some coupling between the B state and NO_2 states, which are not accounted for by the vibronic theory.

The DPDs of the B_{1g} modes are all very similar (Figures 6 and 7) in that they show a constant depolarization ratio of 0.75 in the Soret band region and a maximum with inverse polarization between Q_ν and Q_0. This results from an A_{2g}-type vibronic perturbation (matrix element $c_{QB}^{A_{2g}}$ in Table 1), which, due to Table 1, is indicative of a B_{2g} distortion and/or the combination of ruffling (B_{1u}) and doming (A_{2u}). The same distortions would cause a vibronic A_{1g} perturbation of B_{2g}-type modes, and this is indeed obtained from the DPD of ν_{29}, which becomes nearly polarized in the B band region due to a strong contribution from FC-type coupling ($c_{BB}^{A_{1g}}$) (Figure 5). Ruffling and saddling would give rise to vibronic perturbations of B_{2g} and B_{1g} symmetry of B_{1g} and B_{2g} modes, respectively. This does not change their depolarization ratios. However, a successful fit to the corresponding REPs can only be obtained if these vibronic perturbations are taken into consideration; i.e., $c_{lm}^{B_{1g}}$ and $c_{lm}^{B_{2g}}$ parameters had to be used for the fits to data of all B_{1g}- and B_{2g}-type modes. Unfortunately, this makes the determination of these coupling parameters somewhat less certain since significant correlation effects are unavoidable.

The Raman line at 1361 cm^{-1} was earlier assigned to the NO_2 symmetric stretch. As shown by our normal coordinate analysis, however, this is an oversimplification.[21] In fact, the NO_2 symmetric stretch mixes heavily with $C_\alpha NC_\alpha$ bending and $C_\alpha C_\beta$ stretch. It is therefore not surprising that this mode becomes resonance-enhanced with B and Q band excitation (Figure 4). The DPD and REP were well fitted by our model. Interestingly, the antisymmetric contribution ($c_{QB}^{A_{1g}}$) is small compared with the large contribution obtained for ν_2. This suggests that the mode is less affected by nonplanar distortions.

In accordance with the assignment of Hobbs et al.,[25] our normal coordinate analysis suggests that the band at 1380 cm^{-1} is assignable to ν_4.[21] It turned out, however, that the eigenvector contains contributions from the NO_2 symmetric stretch. One may speculate that this is the reason for our inability to fit the DPD of this band (Figure 8), which is pretty much different from all DPDs of this mode obtained for other porphyrins and heme groups.[19,26,27] As we argue in the discussion, electronic interaction between the NO_2 group and the porphyrin macrocycle causes a breakdown of the four orbital model. It is reasonable to assume that this may particularly affects those modes with strong contributions from NO_2 vibrations.

Taken together, the analysis of our data unambiguously yields that 5,15-NO_2−OEP is subject to out-of-plane ruffling and saddling. Even though the vibronic perturbations obtained do

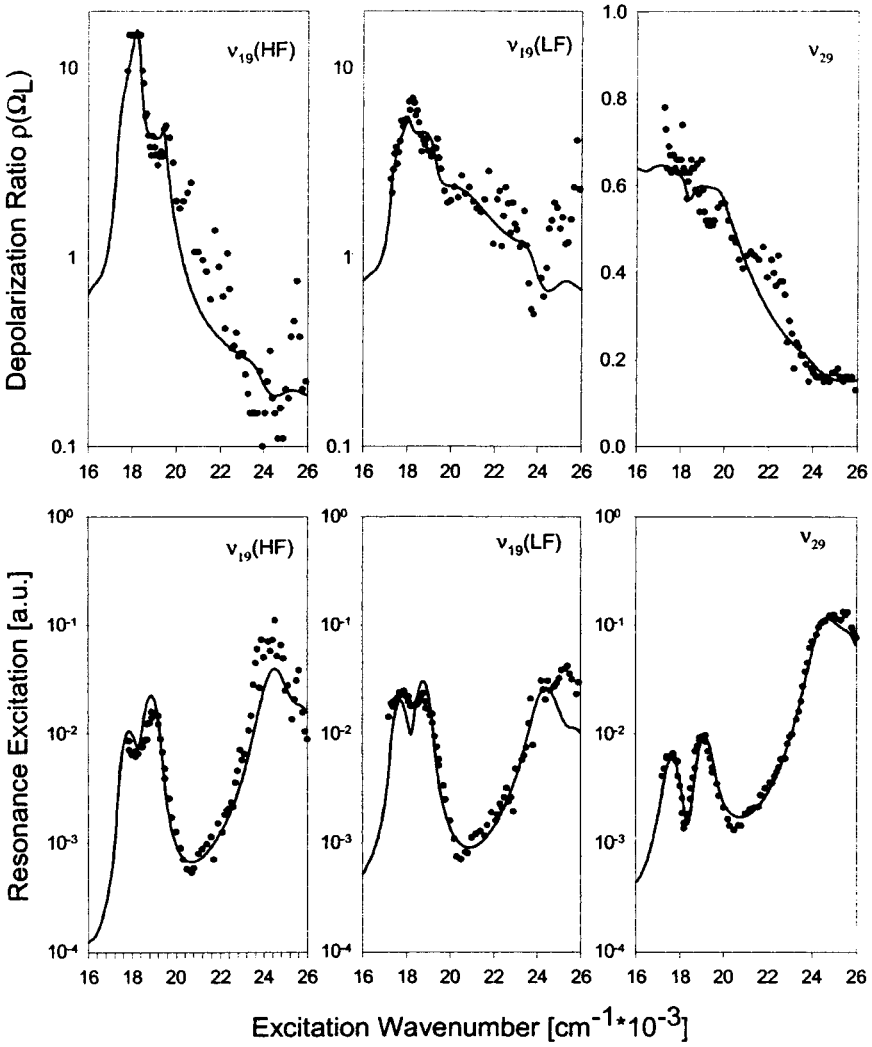

Figure 5. Depolarization dispersion and resonance excitation profiles of the high- and low-frequency subline of the A_{2g}-type ν_{19} and B_{2g}-type ν_{29} vibration of Ni(5,15-NO_2−OEP). The solid lines result from the fitting procedure outlined in Materials and Methods and Results.

not allow the discrimination between B_{2g} and B_{1u}/A_{2u} distortions, we can safely assume at least a very significant contribution from the former since this is exactly the symmetry type, which one derives from the position of the NO_2 groups, which lower the molecule's symmetry per se from D_{4h} to D_{2h}. Our data, however, show that the nitro groups have a significant impact on the structure of the macrocycle. From our earlier studies on Fe−protoporphyrin IX in heme proteins, we know that distortions imposed by the peripheral substituents and the protein environment normally cause moderate perturbations of the Raman tensor so that the coupling matrix elements reflecting the vibronic perturbations are significantly lower than those exhibiting the symmetry of the unperturbed mode.[26,27] Even in MbCN, where the axial ligands give rise to considerable B_{1g}-type distortions, the corresponding matrix elements are still lower than that of the respective vibrational symmetry.[28] In the present case, however, this is no longer true. For ν_{11} and ν_{10}, the NO_2-induced B_{2g} distortions give rise to A_{2g}-type matrix elements, which are comparable with the corresponding B_{1g} coupling parameters (Table 1). Moreover, coupling elements resulting from out-of-plane distortions are also larger than corresponding values of, for instance, Ni(OETPP).[22] This holds in particular for the two ν_2 sublines, for which we obtained $c_{QB}^{A_{2g}} = -166$ and -355 cm^{-1}, whereas only 97 cm^{-1} were obtained for Ni(OETPP).[22] As shown above, this matrix element results from the combined presence of ruffling and saddling.

Discussion

Validity of Fitting Parameters. In what follows, the coupling parameters c_{es}^{Γ} will be used to discuss the various distortions affecting the macrocycle of nitroporphyrins. However, not all parameters obtained are of equal use for this purpose. For the DPDs and REPS of A_{1g} and A_{2g} modes, all $c_{es}^{A_{1g}}$ (es = Q,B), $c_{QB}^{B_{1g}}$, $c_{QQ}^{B_{2g}}c_{QB}^{B_{2g}}$, and $c_{QB}^{A_{2g}}$ values are quite reliable. The Jahn−Teller parameters, $c_{QQ}^{B_{1g}}$, $c_{BB}^{B_{1g}}$, and $c_{BB}^{B_{2g}}$ are likely to additionally reflect some contribution from metal−porphyrin interactions in the ground state[24] and excited-state interaction between macrocycle and nitro groups and are therefore difficult to compare. For the DPDs and REPS of B_{1g} and B_{2g} modes, the correlation between corresponding $c_{QB}^{B_{1g}}$ and $c_{QB}^{B_{2g}}$ parameters may affect their validity, but at least for the B_{1g} modes, we obtained $c_{QB}^{B_{1g}} > c_{QB}^{B_{2g}}$ (Table 1), as expected, since $c_{QB}^{B_{2g}}$ results from the second-order term reflect ruffling and saddling. Therefore, we consider the Herzberg Teller parameters $c_{QB}^{A_{2g}}$ and $c_{QB}^{B_{1g}}$ of B_{1g} modes as reliable. For the B_{2g} mode ν_{29}, all $c_{es}^{A_{1g}}$ of B_{2g} modes are reliable without restriction, while $c_{QB}^{B_{1g}}$ and $c_{QB}^{B_{2g}}$ appear somewhat more affected by correlation effects than the corresponding parameters of the B_{1g} modes investigated. With respect to the evaluation of symmetry lowering distortions, we will use B_{1g} and B_{2g} modes for in-plane B_{2g} distortions (coupling parameters $c_{QB}^{A_{1g}}$, $c_{QB}^{B_{1g}}$, $c_{QQ}^{B_{2g}}$, and$c_{QB}^{B_{2g}}$, respectively) and A_{1g} and

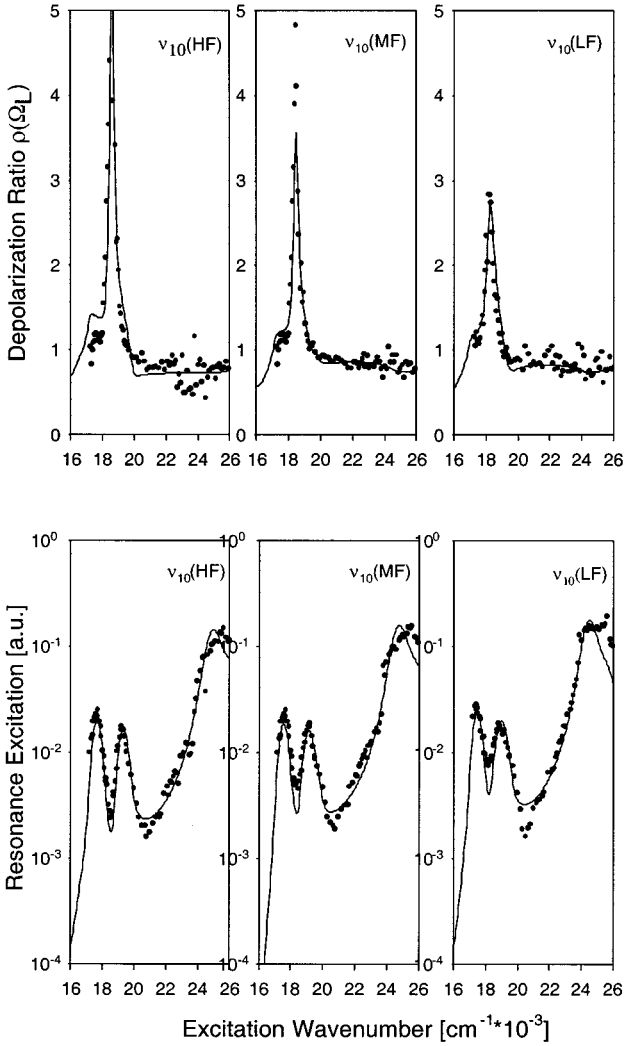

Figure 6. Depolarization dispersion and resonance excitation profiles of the high-, intermediate-, and low-frequency subline of the B_{1g}-type ν_{10} of Ni(5,15-NO_2−OEP). The solid lines result from the fitting procedure outlined in Materials and Methods and Results.

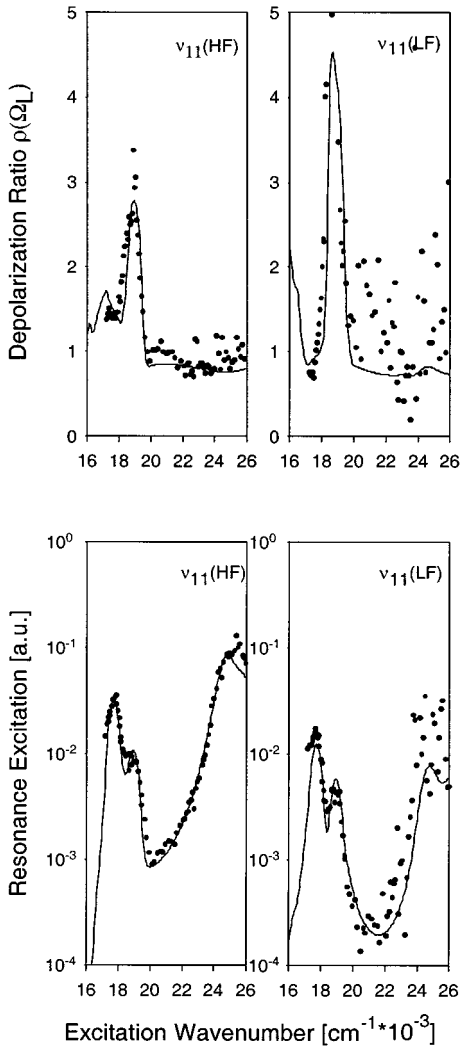

Figure 7. Depolarization dispersion and resonance excitation profiles of the hig-h and low-frequency subline of the B_{1g}-type ν_{11} of Ni(5,-15-NO_2−OEP). The solid lines result from the fitting procedure outlined in Materials and Methods and Results.

A_{2g} modes for out-of-plane B_{1u} and B_{2u} distortions (coupling parameters $c_{QB}^{B_{1g}}$, $c_{QQ}^{B_{2g}}$,$c_{QB}^{B_{2g}}$, and $c_{QB}^{A_{1g}}$, respectively).

The discussion is organized as follows. First, we will show how different information about the ground and excited states geometries can be extracted from the vibronic coupling matrix elements. With this in mind, we then compare the different conformers revealed by our Raman data to identify differences in terms of planar and nonplanar distortions. This is followed by comparison of Ni(5,15 NO_2−OEP) and Ni(5-NO_2−OEP). In the next step, we utilize the vibronic coupling matrix elements and the frequency positions of core size marker modes to quantitatively estimate the out-of-plane distortions of the obtained Ni(5,15 NO_2−OEP) conformers. The results of this analysis are then compared with molecular mechanics calculations. Finally, we report results of some INDO calculations to elucidate the $\pi\pi$ interaction between NO_2 and porphyrin macrocycle.

Interpretation of Coupling Parameters. To obtain information about symmetry lowering distortions from the coupling parameters c_{es}^{Γ}, we have to consider three different contributions. First, these parameters depend on the strength of the respective normal coordinate deformation $\delta\bar{q}^{B_{2g}}$ (eq 8) or, for the out-of-plane distortions, on the product $\delta\bar{q}^{B_{1u}}\delta q^{B_{2u}}$ and potentially also on $\delta\bar{q}^{B_{1u}}\delta q^{A_{2u}}$. Second, they depend on the partial derivative with respect to these distortions and the normal coordinate, i.e., $\partial\hat{H}_{el_0}/(\partial q_r^{\Gamma_r}\partial q^{B_{2g}})$, $\partial\hat{H}_{el}/(\partial q_r^{\Gamma_r}\partial q^{B_{1u}}\partial q^{B_{2u}})$, and $\partial\hat{H}_{el}/(\partial q_r^{\Gamma_r}\partial q^{B_{1u}}\partial q^{A_{2u}})$. Third, electronic perturbations (eq 4) contribute toward c_{es}^{Γ} because these parameters are expressed

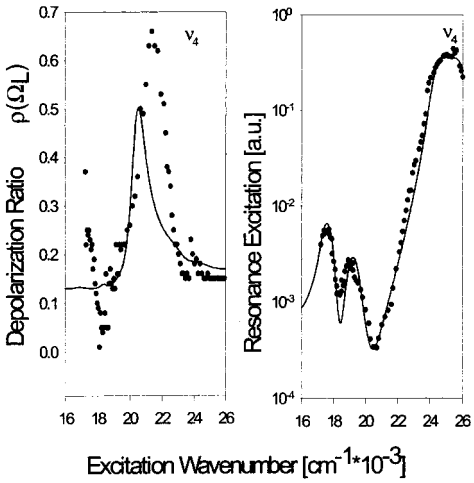

Figure 8. Depolarization dispersion and resonance excitation profiles of the A_{1g}-type ν_4 of Ni(5,15-NO_2−OEP). The solid lines result from the fitting procedure outlined in Materials and Methods and Results.

TABLE 1: (a) Vibronic Coupling Parameters (in cm^{-1}) Obtained from the Fits to the DPDs and REPs of Ni 5,15-Dinitro−OEP[a]

(1) Modes Exhibiting A_{1g} Symmetry in D_{4h}

	$c_{QQ}^{A_{1g}}$	$c_{QB}^{A_{1g}}$	$c_{BB}^{A_{1g}}$	$c_{QQ}^{B_{1g}}$	$c_{QB}^{B_{1g}}$	$c_{BB}^{B_{1g}}$	$c_{QQ}^{B_{2g}}$	$c_{QB}^{B_{2g}}$	$c_{BB}^{B_{2g}}$	$c_{QB}^{A_{2g}}$
ν_2^{HF}	**102**	**−109**	**333**	−	−	−	14	−24	2	−166
ν_2^{LF}	**153**	**−117**	**248**				34	−168	62	−355
ν_2^{HF} [b]	**79**	**202**	**142**				−15	−19	57	−258
ν_4	**−66**	**−252**	**−211**				39	31	80	−
ν_{NO_2}	**−43**	**220**	**−215**				32	−162	−82	59

(2) Modes Exhibiting B_{1g} Symmetry in D_{4h}

	$c_{QQ}^{A_{1g}}$	$c_{QB}^{A_{1g}}$	$c_{BB}^{A_{1g}}$	$c_{QQ}^{B_{1g}}$	$c_{QB}^{B_{1g}}$	$c_{BB}^{B_{1g}}$	$c_{QQ}^{B_{2g}}$	$c_{QB}^{B_{2g}}$	$c_{BB}^{B_{2g}}$	$c_{QB}^{A_{2g}}$
ν_{10}^{HF}	−	−	−	**−671**	**−429**	**−70**	82	263	−255	421
ν_{10}^{MF}	−	−	−	**−650**	**−526**	**18**	119	320	−276	419
ν_{10}^{LF}	−	−	−	**−665**	**−469**	**49**	−20	273	−256	380
ν_{10}^{MF} [b]	−	−	−	**−484**	**−375**	**82**	78	241	−47	189
ν_{11}^{LF}	−	−	−	**−669**	**−149**	**176**	206	93	−24	400
ν_{11}^{HF}	−	−	−	**−24**	**−341**	**−64**	−33	120	−39	310

(3) Mode Exhibiting B_{2g} Symmetry in D_{4h}

	$c_{QQ}^{A_{1g}}$	$c_{QB}^{A_{1g}}$	$c_{BB}^{A_{1g}}$	$c_{QQ}^{B_{1g}}$	$c_{QB}^{B_{1g}}$	$c_{BB}^{B_{1g}}$	$c_{QQ}^{B_{2g}}$	$c_{QB}^{B_{2g}}$	$c_{BB}^{B_{2g}}$	$c_{QB}^{A_{2g}}$
ν_{29}	−111	0	−142	−18	−267	18	**−60**	**−241**	**−31**	−

(4) Mode Exhibiting A_{2g} Symmetry in D_{4h}

	$c_{QQ}^{A_{1g}}$	$c_{QB}^{A_{1g}}$	$c_{BB}^{A_{1g}}$	$c_{QQ}^{B_{1g}}$	$c_{QB}^{B_{1g}}$	$c_{BB}^{B_{1g}}$	$c_{QQ}^{B_{2g}}$	$c_{QB}^{B_{2g}}$	$c_{BB}^{B_{2g}}$	$c_{QB}^{A_{2g}}$
ν_{19}^{HF}	−70	−42	−128	−252	132	−8	−	−	−	**−716**
ν_{19}^{LF}	−4	−91	−55	−159	−368	−042				**−710**

(b) Electronic Parameters (in cm^{-1}) Obtained from the Fits to the DPDs and REPs of 5,15-Dinitro-Ni(OEP)

δA_{1g}	−1500
Γ_Q	130
Γ_B	530
σ_Q	180
σ_B	180

[a] The values of the coupling parameters exhibiting the corresponding D_{4h} symmetry are typed in bold [b] Ni 5-nitro−OEP.

in terms of the perturbed electronic wave functions of the distorted molecule.[18,26] Since the absorption spectra do not allow us to separately determine the electronic distortions (contrary to B_{1g} perturbations, electronic B_{2g}- and A_{2g}-type perturbations have to be very strong in order to cause significant splitting between the *x* and *y* components of the B and Q state[19]), we have no independent knowledge of their contribution to the c_{es}^{Γ}. These three contributions will be considered in the subsequent discussion.

Comparison of Different Conformers. Our spectral analysis of the ν_{10} band shape of Ni(5,15-diNO_2−OEP) revealed three different sublines at 1633 cm^{-1} (ν_{10}^{LF}), 1642 cm^{-1} (ν_{10}^{MF}), and 1652 cm^{-1} (ν_{10}^{HF}), assignable to coexisting conformers which in the following are denoted as CP_1, CP_2, and CP_3, respectively. Only two sublines could be identified for the three other structure-sensitive lines investigated, namely, ν_2, ν_{19}, and ν_{11}. All these lines are well-known to downshift with increasing nonplanar distortions.[29] A comparison of the intensities suggests that for ν_2 and ν_{19}, the more intense lower-frequency sublines at 1591 and 1571 cm^{-1} result from overlapping contributions from CP_1 and CP_2, whereas the higher-frequency subline is assignable to CP_3. The situation is somewhat different for ν_{11}, for which the high-frequency subline is more intense. This suggests that it represents two overlapping sublines from conformers assignable to CP_2 and CP_3. The DPDs of all these sublines show that all three conformers are subject to in-plane (B_{2g}), out-of-plane B_{1u} (ruffling), B_{2u} (saddling), and possibly also A_{2u} (doming) distortions.

To assess the out-of-plane distortions in the different conformers, we first compare the data for the sublines of ν_2. From the coupling constants in Table 1, one derives $c_{QB}^{A_{2g}}/c_{QB}^{A_{1g}}$ values of 3.03 for ν_2^{LF} (CP1 and CP2) and 1.5 for ν_2^{HF} (CP3). This difference is significant and indicates that the CP1/CP2 are more nonplanar than CP3. This notion is in accordance with Raman spectroscopy data on numerous nonplanar porphyrins, which suggest that in particular ruffling causes all the so-called core size marker modes to downshift.[7,29]

The coupling parameters of the A_{2g}-type mode ν_{19} are more difficult to interpret. For the ratio $c_{QB}^{A_{1g}}/c_{QB}^{A_{2g}}$, one obtains 0.13 for ν_{19}^{LF} (CP1) and 0.05 for ν_{19}^{HF}. This underscores the notion that the CP1/CP2 are more nonplanar than CP3. On the contrary, the Franck−Condon parameters $c_{QQ}^{A_{1g}}$ and $c_{BB}^{A_{1g}}$ are significantly larger for ν_{19}^{HF} than for ν_{19}^{LF}. This can be interpreted as resulting from differences between the electronic part $\langle e|\partial^3\bar{H}_{el}/\partial q_r^{A_{2g}}\,\partial q^{B_{1u}}\,\partial q^{B_{2u}}|e\rangle (e = Q, B)$ rather than from differences in the product $\delta\bar{q}^{B_{1u}}\delta q^{B_{2u}}$ in the matrix elements $c_{ee}^{A_{1g}}$. Hence, our data indicate that the excited states are distorted along the normal coordinate of ν_{19} and that this antisymmetric distortion is more pronounced for CP3 than for CP1/CP2.

We now discuss the coupling parameters arising from B_{2g} and potentially also from the combined presence of B_{1u} and A_{2u} distortions. To compare them for different conformers, we normalized them onto the corresponding parameter obtained for the D_{4h} symmetry to eliminate uncertainties of the determination of the relative concentrations. For ν_{10}, the respective ratios $c_{QB}^{A_{2g}}/c_{QB}^{B_{1g}}$ are 0.57, 0.64, and 0.62 for CP1, CP2, and CP2, respectively. This suggests that the distortions which gives rise to $c_{QB}^{A_{2g}}$ are very similar for the three conformers. On the contrary, the corresponding ratios are quite different for ν_{11}^{LF} and ν_{11}^{HF}, i.e., 2.68 and 0.91, respectively. The latter finding suggests that CP1 and CP2/CP3 differ in terms of NO_2 orientation, which, as we will show below, determines the degree of $\pi\pi$ mixing between the NO_2 p_z and the macrocycle a_{2u} orbital. This interaction gives rise to B_{2g} distortion. The larger $c_{QB}^{A_{2g}}/c_{QB}^{B_{1g}}$ (ν_{11}) value observed for CP1 thus results from a stronger B_{2g} distortion induced by more horizontally oriented NO_2 groups. This explanation, however, is at odds with the nearly identical $c_{QB}^{A_{2g}}/c_{QB}^{B_{1g}}$ values of the ν_{10} sublines, since it is difficult to imagine that a mode with such a strong $C_\alpha-C_m$ stretching contribution remains unaffected by the $\pi\pi$ interaction between NO_2 and macrocycle. Alternatively, one can invoke the possibility that a significant part of $c_{QB}^{A_{2g}}$ results from the combined presence of ruffling (B_{1u}) and doming (A_{2u}). The corresponding contribution to the vibronic perturbation is proportional to $\delta\bar{q}^{A_{2u}}\delta\bar{q}^{B_{1u}}$. If CP 1, as expected, is more ruffled and/or more domed than CP2 and CP3, one indeed expects that $c_{QB}^{A_{2g}}$ (CP1) > $c_{QB}^{A_{2g}}$ (CP2/CP3), as observed for ν_{11}. The different behavior of the corresponding ν_{10} subline parameters then reflects a negligibly small contribution of $\partial^3\bar{H}_{el}/(\partial q_r\partial q^{A_{2u}}\partial q^{B_{1u}})$ to the vibronic perturbation of ν_{10}. This is not unlikely, since changes in the doming coordinate may have a limited influence on $C_\alpha-C_m$ stretch. Overall, this model predicts that the three conformers exhibit comparable B_{2g}-type distortions (and thus similar NO_2-orientations) but differ in terms of nonplanarity.

The $c_{QB}^{B_{1g}}$ and $c_{QB}^{B_{2g}}$ parameters of ν_{19} and ν_2, respectively, also deserve some comments. They both reflect also the influence of B_{2g} and, possibly, A_{2u} distortions. Though their values are less reliable than those of the $c_{QB}^{A_{2g}}$ parameters obtained from the ν_{10} and ν_{11} data, the differences between the corresponding low- and high-frequency sublines must be considered as significant. They consistently indicates that CP1/CP2 is more affected by

the corresponding distortions than CP3, consistent with the results obtained for the ν_{11} sublines. Thus, this finding is consistent with the notion that CP1 is more affected by doming and ruffling than CP2 and CP3

Taken together, the model most consistent with our experimental data can be described as follows. The three coexisting conformers obtained from our spectral analysis are all subject to in-plane B_{2g} deformations and out-of-plane ruffling (B_{1u}) , saddling (B_{2u}), and doming (A_{2u}). The conformer CP1 assignable to the lower-frequency subline of the marker bands ν_2, ν_{10}, ν_{11}, and ν_{19} is more nonplanar (most likely more ruffled) than the conformers CP2 and CP3 giving rise to the middle- and high-frequency sublines. The B_{2g} deformations of the three conformers are likely similar. One therefore expects that they exhibit similar NO_2 orientations.

Comparison of Ni(5,15-NO_2−OEP) with Ni(5-NO_2−OEP). Unfortunately, the REPs and DPDs of Ni(5-NO_2−OEP) are of much lower quality. The large noise does not allow a quantitative analysis of most REPs and DPDs. To facilitate at least a rough comparison between Ni(5-NO_2−OEP) and (5,15-NO_2−OEP), we have carried out a fit to the REPs and DPDs of the sublines ν_{10}^{MF} and ν_2^{HF}. To simulate the multimode contribution, we used the coupling parameters obtained for Ni(5,15-diNO_2−OEP). The result of this analysis is shown in Figure 9. The fit to the REP of ν_2^{HF} does not accurately account for the very scattered Q_0-intensities, but reproduces the DPDs with sufficient accuracy, whereas a satisfactory reproduction of the data is obtained for ν_{10}^{MF}. The coupling parameters are also listed in Table 2. Apparently, the relative and absolute $c_{QB}^{B_{2g}}(\nu_2^{HF})$ and $c_{QB}^{A_{2g}}(\nu_{10}^{MF})$ values, which reflect B_{2g}-type distortions, are smaller than the corresponding coupling parameters of Ni(5,15-diNO_2−OEP). This indicates, that in accordance with expectation, B_{2g} distortions are weaker in Ni(5-NO_2−OEP). The absolute value for $c_{QB}^{A_{2g}}(\nu_2^{HF})$ is larger than that obtained for the ν_2^{HF} of Ni(5,-15-diNO_2−OEP), but its relative value $c_{QB}^{A_{2g}}/c_{QB}^{A_{1g}} = 1.2$ is even lower. This suggests that Ni(5-NO_2−OEP) is less nonplanar than Ni(5,15-diNO_2−OEP), in accordance with conclusions drawn from earlier Raman experiments.[25] Altogether, this comparison supports the validity of the analysis based on our Raman dispersion data.

Estimation of Macrocycle Deformations. The crystal structure of Ni(OETPP) revealed a very strong saddling B_{2u}-type distortion along the γ_{18} mode, which adds to a total value of 3.8 Å and a hardly detectable small ruffling B_{1u} distortion of 0.09 Å.[30] Raman dispersion spectroscopy confirmed the existence of saddling and ruffling for Ni(OETPP) in CS_2.[22]

A comparison of the $c_{QB}^{A_{2g}}$ values of the two ν_2 sublines of Ni(5,15-diNO_2−OEP) (−166 and −355 cm^{-1}) and the (single) ν_2 line of Ni(OETPP) (97 cm^{-1})[22] suggests that the former molecule is much more nonplanar than the latter. This seems to be surprising because the core size marker bands of the Raman spectrum appear much more downshifted for Ni(OETPP).[31] The absorption spectrum also indicates that Ni(OETPP) is superior in terms of nonplanarity. However, this contradiction can easily be resolved if one takes into account that $c_{QB}^{A_{2g}}$ linearly depends on the product $\delta\bar{q}^{B_{1u}}\delta q^{B_{2u}}$. On the contrary, the frequencies of the marker lines exhibit a nonlinear dependence on the total amount of ruffling ($\Delta_{B_{1u}}$) and saddling ($\Delta_{B_{2u}}$), which according to Franco et al. can be approximated by[7]

$$\Omega = a_1 + b_1\Delta_{B_{1u}}^4 + a_2 + b_2\Delta_{B_{2u}}^4 \qquad (9)$$

where a_1, a_2, b_1, and b_2 have characteristic values for each of the marker lines. To employ eq 9 for a comparison of Ni(OETPP) and Ni(5,15-diNO_2−OEP), we use the planar conformer of Ni(OEP) as a reference system so that the $a_1 = a_2 = 1608$ cm^{-1}, which is somewhat higher than the values used by Franco et al.[7] To estimate b_1, we use the $\Delta_{B_{1u}} = 1.5$ Å obtained for crystallized triclinic Ni(OEP)[12] and the corresponding Raman frequency of 1595 cm^{-1}[32] to obtain $b_1 = 2.56$ cm^{-1}/Å^4. The coefficient can be estimated to 0.215 cm^{-1}/Å^4 from the ν_2 frequency of Ni(OETPP) (1563 cm^{-1}) and the $\Delta_{B_{2u}} = 3.8$ Å value of its crystal structure.

To estimate Δ_{ruf} and Δ_{sad} for Ni(5,15-diNO_2−OEP), we compare its $c_{QB}^{A_{2g}}(\nu^2)$ values (Table 1) with that of Ni(OETPP). By assuming that the electronic part of the vibronic coupling matrix element is identical for both molecules, one obtains

$$\delta\bar{q}^{B_{1u}}\delta\bar{q}^{B_{2u}}(\nu_2^{HF},5,15-NO_2-NiOEP) = 1.82\delta\bar{q}^{B_{1u}}\delta\bar{q}^{B_{2u}}(\nu_2,\ NiOETPP)$$

$$\delta\bar{q}^{B_{1u}}\delta\bar{q}^{B_{2u}}(\nu_2^{LF},5,15-NO_2-NiOEP) = 3.9\delta\bar{q}^{B_{1u}}\delta\bar{q}^{B_{2u}}(\nu_2,\ NiOETPP) \qquad (10)$$

$\delta\bar{q}^{\Gamma}$ is a mass-weighted normal coordinate. If it is predominantly determined by a single normal coordinate (normally that of the

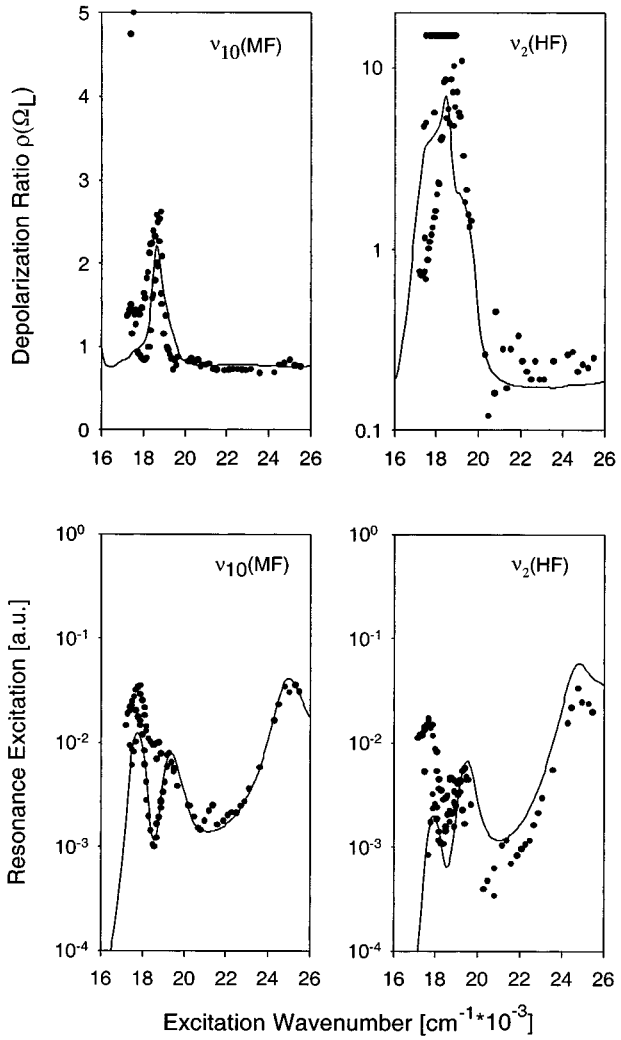

Figure 9. Depolarization dispersion and resonance excitation profiles of the intermediate frequency subline of the B_{1g}-type ν_{10} and high-frequency subline of the of the A_{1g}-type ν_2 vibration of Ni(5-NO_2−OEP). The solid lines result from the fitting procedure outlined in Materials and Methods and Results.

TABLE 2: Results from the SNCD Analysis of All Ni(5,15-NO_2−OEP) and Ni(5-NO_2-NO_2−OEP) Conformers with a Boltzmann Factor of at Least 5% at Room Temperature[a]

(a) Ni(5,15-NO_2−OEP)

relative energy	ruffling	doming	saddling	rhombic	Boltzmann factor[b]	substituent orientation[c]
0	2.130	0.613	0.183	0.310	0.26	αα$\beta\beta$-Nh+αα$\beta\beta$-Nh+
1.0	2.016	0.436	0.094	0.193	0.046	αα$\beta\beta$-Nh+αα$\beta\beta$-Nv+
0	2.113	0.623	0.003	0.303	0.26	αααα-Nh+$\beta\beta\beta\beta$-Nh+
0.2	2.131	0.605	0.089	0.298	0.19	αα$\beta\beta$-Nh+$\beta\beta$αα-Nh+
0.76	2.131	0.399	0.0	0.187	0.075	αα$\beta\beta$-Nh+$\beta\beta$αα-Nv-

(b) Ni(5-NO_2−OEP)

relative energy	ruffling	doming	saddling	rhombic	Boltzmann factor[b]	substituent orientation[c]
0	1.710	0.313	0.078	0.145	0.19	αααα-Nh+$\beta\beta\beta\beta$
0	1.657	0.101	0.073	0.003	0.19	αα$\beta\beta$-Nh+$\beta\beta$αα
0.1	1.715	0.308	0.168	0.143	0.15	αα$\beta\beta$-Nh+αα$\beta\beta$
0.61	1.656	0.093	0.008	0.080	0.66	αβαβ-Nh+αβαβ

[a] The first column lists the relative energies (in kcal/mol with respect to the conformer of lowest energy). The SNCD values (in Å) were obtained by using a complete basis set; i.e., the deformations are summed over all modes of a given symmetry. Since it is calculated from the individual distortions by use of eq 16, the sign has become arbitrary and is therefore omitted. As we have outlined in the text, the predominant contributions for all deformations are provided by distortions along the modes of lowest and second lowest frequency. The right-hand column depicts the orientation of the substituents. [b] The Boltzmann factor is normalized on the partition sum of the system to yield the molar fraction of the conformer. [c] Oriented above (α) and below (β) the average plane of the macrocycle; h, horizontal orientation; v, vertical orientation; oriented above (+) and below (−) the average plane

lowest frequency mode of symmetry Γ), it can be calculated by[22]

$$\delta\bar{q}^{\Gamma} = \sqrt{\sum_i m_i(\Delta_i^r)^2} \qquad (11)$$

where Δ_i and m_i are the out-of-plane displacement and mass of the ith atom. The total distortion for a distinct symmetry Γ is then given by

$$\Delta_{\Gamma} = \sqrt{\sum_i (\Delta_i^{\Gamma})^2} \qquad (12)$$

If one neglects the small mass difference between the nitrogen and carbon, it follows from eqs 9−12 that

$$\Delta_{B_{1u}}\Delta_{B_{2u}}(\nu_2^{\mathrm{HF}},5,15\text{-}NO_2\text{-}NiOEP) = 1.82\Delta_{B_{1u}}\Delta_{B_{2u}} \quad (\nu_2, \mathrm{NiOETPP})$$

$$\Delta_{B_{1u}}\Delta_{B_{2u}}(\nu_2^{\mathrm{LF}},5,15-NO_2-NiOEP) = 3.9\Delta_{B_{1u}}\Delta_{B_{2u}} \quad (\nu_2, \mathrm{NiOETPP}) \qquad (13)$$

provided that the out-of-plane modes exhibit similar eigenvectors for these two molecules. To obtain $\Delta_{B_{1u}}$ and $\Delta_{B_{2u}}$ for Ni(5,15-diNO$_2$−OEP), we combine eqs 9 and 13 and obtain

$$b_2(\Delta_{B_{1u}})^8 - \frac{\Omega(\nu_2)}{b_2}(\Delta_{B_{2u}})^4 + \frac{a+b\eta^4}{b_2} = 0 \qquad (14)$$

where $\Omega(\nu_2)$ is the wavenumber of the ν_2 line of Ni(5,15-diNO$_2$−OEP) and η = 1.82 and 3.9 for ν_2^{HF} and ν_2^{LF}, respectively. Solving eq 16 yields two different pairs of values for both sublines, i.e., (1) $\Delta_{B_{1u}} = \pm 1.67$ Å, $\Delta_{B_{2u}} = \pm 0.37$ Å, and $\Delta_{B_{1u}} = \pm 0.21$ Å, $\Delta_{B_{2u}} = \pm 2.98$ Å for ν_2^{HF} (representing CP3) and (2) $\Delta_{B_{1u}} = \pm 1.72$ Å, $\Delta_{B_{2u}} = \pm 0.77$ Å, and $\Delta_{B_{1u}} = \pm 0.31$ Å, $\Delta_{B_{2u}} = \pm 3.21$ Å for ν_2^{LF} (representing CP1/CP2). If, as suggested by the above considerations, the macrocycle also exhibits some significant contributions from doming, one has to rule out the solution with the stronger saddling component because one would then also expect some contributions from the third-order term $(\partial\hat{H}_{\mathrm{el}}/\partial q_r \partial\bar{q}^{A_{2u}}\partial\bar{q}^{B_{2u}})\delta\bar{q}^{A_{2u}}\delta\bar{q}^{B_{2u}}$ (B_{1g} perturbation) to the vibronic coupling of the B_{1g} and B_{2g} modes, in contrast to our experimental data.

Altogether, the above calculations and considerations led us to conclude that both conformers are mostly ruffled, with some minor degree of saddling and with some not yet quantified contribution from doming.

Molecular Mechanics Calculations. To obtain independent information about the structural heterogeneity of the investigated porphyrins, we have performed molecular mechanics calculations to obtain all stable conformers (local minima with respect to all normal coordinates) of Ni(5,15-diNO$_2$−OEP). These conformers differ in terms of their substituent orientations. The thus obtained structures were then subjected to a SNCD analysis as developed by Jentzen et al.[15] in order to obtain all symmetry classified distortions. Table 2a lists the relative energies (with respect to the conformer for which the lowest energy was obtained) and the SNCD values of all conformers with a Boltzmann factor of at least 5% at room temperature. A more complete list of conformers and their energies and SNCDs are given in the Supplementary Information (Table S2) for this paper.

The most interesting aspects of these results are as follows:
1. The most stable conformers in the (relative) energy range between 0 and 0.2 kcal/mol all exhibit very strong ruffling (>2 Å) and significant doming (∼0.5 Å). Saddling is comparatively weak (between 0 and 0.21 Å). Waving and propellering are even less relevant. As physically expected, the dominant contributions to all these distortions result from deformations along the normal coordinates of the lowest-frequency mode (Figure 1) of the respective symmetry block (minimal basis).
2. All conformers exhibit significant B_{2g}-type deformations. They are particularly large for the conformers of lowest energy (∼0.3 Å). As assumed as a basis for our theoretical considerations, contributions from other asymmetric in-plane distortions are negligibly small. The totally symmetry A_{1g}-type deformation, however, is large (>0.75 Å with respect to the reference system Cu(II)−porphyrin). Surprisingly, the dominant contribution to

the total B_{2g} distortion results from deformations along the normal coordinates of the B_{2g} vibrations with the second lowest frequency (ν_{34}) (extended basis set in Table 2a). The lowest-frequency mode ν_{35} is only of minor relevance. The eigenvector of ν_{34} is shown in Figure 1. This mode involves a rhombic distortion along the Ni−C_m lines, NO_2 symmetric bending, and some ethyl deformation.

3. All three conformers in the 0−0.2 kcal/mol energy range exhibit different ethyl orientations, i.e., $\alpha\alpha\beta\beta$-Nh+-$\alpha\alpha\beta\beta$-Nh+, $\alpha\alpha\alpha\alpha$-Nh+-$\beta\beta\beta\beta$-Nh+, and $\alpha\alpha\beta\beta$-Nh+-$\beta\beta\alpha\alpha$-Nh+ (α, above the average plane; β, below the average plane), but the same horizontal (h+) orientation of the NO_2 groups. Conformers with alternating ethyl orientation ($\alpha\beta\alpha\beta$) and vertical NO_2 orientations are not very much populated at room temperature.

In accordance with our interpretation of the Raman data, the SNCD analysis of the theoretically obtained structures support the existence of significant doming. To estimate its contribution to matrix elements of vibronic perturbation, we focus again on the $c_{QB}^{A_{2g}}$ coupling elements of B_{1g} modes. The second-order contribution is proportional to $\Delta^{B_{2g}}$ (≈0.3 Å), whereas the third-order term is related to the product $\Delta^{A_{2u}}\Delta^{B_{1u}} \approx 2.1$ Å × 0.5 Å = 1.05 Å^2 (cf. eq 11). The electronic part of the third-order term, $\langle Q|\partial^3\bar{H}_{el}/\partial q_r\,\partial q^{A_{2u}}\,\partial q^{B_{1u}}|B\rangle$, can be assumed to be an order of magnitude smaller than that of the second order term, $\langle Q|\partial^2\bar{H}_{el}/\partial q_r\,\partial q^{B_{2g}}|B\rangle$. Thus, the third order term may contribute approximately 25% to the overall strength of $c_{QB}^{A_{2g}}$. This, however, heavily depends on the vibrational mode. Our Raman data indicate that the vibronic perturbation of ν_{11} depends significantly on doming, while this type of distortion is nearly irrelevant for ν_{10}.

Unfortunately, the results of the molecular mechanics calculations do not allow us to make an unambiguous assignment of the observed sublines. The relative energies listed in Table 2a suggest that only four of the calculated conformers (subset I) are significantly occupied at room temperature (between 19% and 26 %). They are very similar with respect to ruffling and in-plane-rhombic distortions, which only vary in the ranges of 2.11−2.13 and 0.3−0.31 Å, respectively. Changes along the doming coordinate are somewhat more pronounced, e.g., 0.52−0.62 Å. All these variations are certainly too small to cause any significant frequency differences. The saddling coordinate varies between 0 and 0.18 Å, but the structural markers are generally not sensitive to such a small amount of saddling.[7] Conformers of second subset (subset II), which are somewhat less nonplanar ($\Delta_{B_{1u}} = 2.016$ and 2.047 Å, $\Delta_{B_{2u}} = -0.094$ and 0.016 Å, and $\Delta_{A_{2u}} = 0.436$ and 0.343 Å), have relative occupations of less than 10% because they separated by more than 2*RT* from the conformer with the lowest energy. Our measurements of Raman spectra at 170 K are not indicative of any significant changes of intensity rations of corresponding sublines.[33] This suggests that the conformers CP1, CP2, and CP3 are nearly isoenergetic. It is therefore more likely that the three conformers in subset I are those detected in our Raman experiments. Due the strong dependence of the marker line frequency on the ruffling distortions, a slightly larger variation of $\Delta_{B_{2u}}$ would already be sufficient to explain the observed frequency differences between the sublines. The different vibronic perturbation parameters arising from nonplanar distortions most likely reflect different contributions from saddling and doming; i.e., CP1/CP2 are less saddled and domed than CP3.

It is of interest to no note that the energy differences between the lowest conformers of the investigated molecules are smaller than *kT*; i.e., they are nearly isoenergetic. A comparison of recent molecular mechanics[34] and DFT calculations on NiTPP[35] suggests that the former might even slightly overestimate the energy differences between two porphyrin conformers.

The magnitude of the distortions derived from the SNCD analysis of the most stable structures is in qualitative agreement with the above estimation from our Raman data. The quantitative discrepancy (20% for the ruffling distortion) may in part result from the assumption that the electronic part of the matrix element $c_{QB}^{A_{2g}}$ is the same for NiOETPP and Ni(5,15-diNO_2−OEP). In view of the electronic interaction between nitro and macrocycle a_{2u} orbitals, this is certainly an oversimplification. However, it is also likely that the conformers are somewhat more saddled than indicated by the SNCD analysis. A saddling of zero as obtained for one of the most stable conformers is not in agreement with the Raman data. Finally, our analysis may somewhat underestimate the influence of ruffling on the ν_2 frequency. As recently shown by Song et al.,[8] several of the "core size markers" exhibit a stronger dependence on ruffling for di-meso substituted than for tetra-meso substituted metalloporphyrins. This may be caused to the presence of doming distortions in the former.

We have also carried out molecular mechanics and SNCD calculations for Ni(5-NO_2-NiOEP). The distortion parameters of the four conformers with the lowest energy are listed in Table 2b. As for Ni(5,15-diNO_2−OEP), one obtains dominant ruffling, followed by doming and a small contribution from saddling. B_{2g} deformations were obtained for three of the conformers. The absolute values of all distortion values are lower than those obtained for Ni(5,15-diNO_2−OEP). This is in full accordance with our Raman data. In fact, the $c_{QB}^{A_{2g}}$ value obtained for the MF-subline of ν_{10} and the SNCD analysis both suggest that the B_{2g} deformation of Ni(5-NO_2−OEP) is approximately half of that of Ni(5,15-diNO_2−OEP). The in-plane distortions induced by the nitro substituents can therefore be considered as additive.

It is interesting to compare the above results with the structure of the fully substituted Ni(5,10,15,20-NO_2−OEP). As recently shown by Senge,[1] the steric demand of NO_2 substituents is comparable with that of the phenyl substituent so that the crystallized tetranitro-substituted macrocycle exhibits strong saddling ($\Delta_{B_{2u}} = 3.35$ Å) with some admixture of ruffling ($\Delta_{B_{1u}} = 0.653$ Å). This shows that type and magnitude of out-of plane distortions does not only depend on the choice of the substituents but also on their number and on the overall symmetry of their attachment.

It should be mentioned that the combined occurrence of doming and ruffling seems to be a characteristic property of 5,15-meso substituted porphyrins. Song et al.[8] and Jentzen et al.[15] have performed SNCD-analyses for a variety of such porphyrins and found that their most stable conformers are domed and ruffled with some contribution form saddling. The authors called this a gabled distortion. Most of the investigated porphyrins (with propyl, isopropyl, and phenyl as meso substituents) are significantly less nonplanar than the nitro substituted porphyrins investigated in the current study. Only Ni(II)-(5,15-di-*tert*-butyl-porphyrin) appears highly non planar with ruffling and doming values in the range of Ni(5,15-diNO_2−OEP). In other words, the nitro groups have approximately the same destabilizing affect on the porphyrin macrocycle as the much more sterically demanding substituent *tert*-butyl.

Thus far, limited attention has been paid to in-plane distortions of porphyrins in solution and in proteins. In part, this stems from the fact that they are more difficult to quantify. Senge et al.[36] have carried out the conformational analysis of a series of decasubstituted free base and Ni(II)−porphyrins with 5,15-diaryl

and 5,15-dialkyl substituents (ethyl, phenyl, and C_6H_3-2,5-O-CH_3) and found a rhombic B_{2g} distortion in the free as well as in the metal compounds. The values obtained (0.09−0.2 Å) for the latter, however, are smaller than that obtained for Ni(5,15-diNO_2−OEP) in the present study. Jentzen et al.[15] observed a somewhat larger B_{2g}-distortion for Ni(5,12-*tert*-butyl-porpyrin) (0.261 Å). This comparison underscores the notion that NO_2 is very effective in reducing the in-plane symmetry of the macrocycle.

A recent mass spectroscopy analysis of 5-NO_2−OEP has revealed a novel fragmentation pathway that involves the cleavage of the porphyrin macrocycle.[37] Such a destruction of the macrocycle was not obtained for β-substituted porphyrins. The authors hypothesized that nonplanar distortions are responsible for the fragmentation of the macrocycle. In view of the present study one may suspect that the in-plane B_{2g} distortion must also be taken into consideration. As shown in Figure 1, this distortion involves a deformation of the $C_\alpha C_m C_\alpha$ angles of the substituted methine bridges, which might facilitate the observed porphyrin scission. This issue can be clarified by comparing metalporphyrins with meso nitro and alkyl substitutions.

Taken together, the molecular mechanics calculations support the results obtained from the analysis of the Raman data in that they provide evidence that both Ni(5,15-diNO_2−OEP) and Ni-(5-NO_2−OEP) are subject to ruffling, doming, and rhombic and, to a minor extent, saddling distortions. This demonstrates that meso substituted nitro groups can very efficiently perturb the symmetry of the porphyrin macrocycle.

INDO/s Calculations. In the above paragraph, we have invoked $\pi\pi$ interaction between NO_2 and porphyrin as the main cause for the symmetry deformations of the macrocycle. To verify this hypothesis, we have performed single-point INDO/S calculations with configuration (CI) interaction for one of the two most stable conformers of Ni(5,15-diNO_2−OEP). Enough orbitals were included in the CI calculations to account for at least 80% of each nickel d orbital. Figures 10 and 11 exhibit the molecular orbitals of three HOMOs (highest occupied orbitals) and three LUMOs (lowest occupied orbital). The highest-lying HOMO 0 is reminiscent of the a_{1u} orbital of the four-orbital model.[23] HOMO 1 is the next lower-energy orbital; it shows the p_z orbitals of the horizontal nitro groups heavily mixed with the a_{2u} orbitals of the macrocycle. This $\pi\pi$ interaction causes a strong electronic perturbation of the ground state. This electronic perturbation causes a structural change and lowering of the symmetry, which might not be fully accounted for in the molecular mechanics calculations. The three LUMOs 0, 1, and 2 nicely demonstrate the interaction between the e_g orbitals of the porphyrin and higher-lying NO_2 orbitals. Because of the 5,15-substitution, only e_{gx} or e_{gy} (depending on the choice of the coordinate system) can mix with NO_2 orbitals. This yields the LUMOs 1 and 2. The other e_g orbital has a node at the substituted meso carbons and remains unaffected. As a consequence, the degeneracy of the e_g LUMOs is removed. Moreover, it becomes clear that the four-orbital model breaks down for nitroporphyrins. This is in accordance with what is indicated also by our Raman data.

The orbital mixing just described results in near-infrared absorption bands appearing in the region between 800 and 1200 nm with intensities that depend on how horizontal the nitro group is with respect to the porphyrin mean plane. The intensities range from a significant fraction of the calculated intensity of the Q band to several times larger than that of the Q band. The bands arise from transitions from the HOMOs

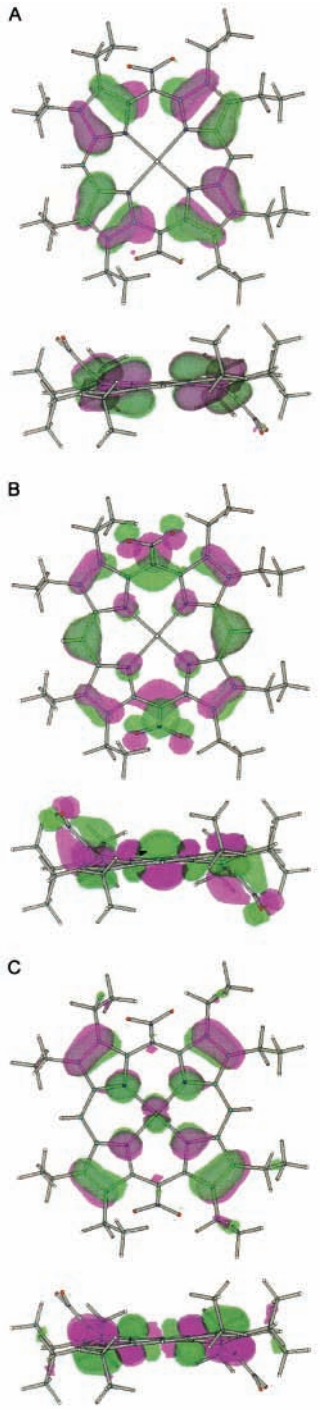

Figure 10. Horizontal and vertical views of three HOMOs of Ni(5,15-NO_2−OEP), as obtained from INDO calculations.

shown to the lowest LUMO, and they have significant porphyrin-to-nitro charge-transfer character. PM3 (for Ni(5,15-diNO_2−OEP)) and low-level ab initio (H_2(5,15-NO_2−OEP)) calculations also predict these near-IR bands, as well as the mixing of the nitro and frontier porphyrin orbitals. However, the predicted bands have not been observed in preliminary spectra of the near-IR region (Medforth, C. J.; Shelnutt, J. A. Unpublished results.). We speculate that the transitions may actually be shifted into the visible region and obscured by the much stronger porphyrin transitions (Q_0 band), but our REPs do not indicate the presence of another resonance energy in the Q band, which, if it exists, should particularly affect ν_{NO_2}. The failure to detect these near-IR bands may indicate that the conformers with the horizontal orientation of the nitro group may actually be at higher energy

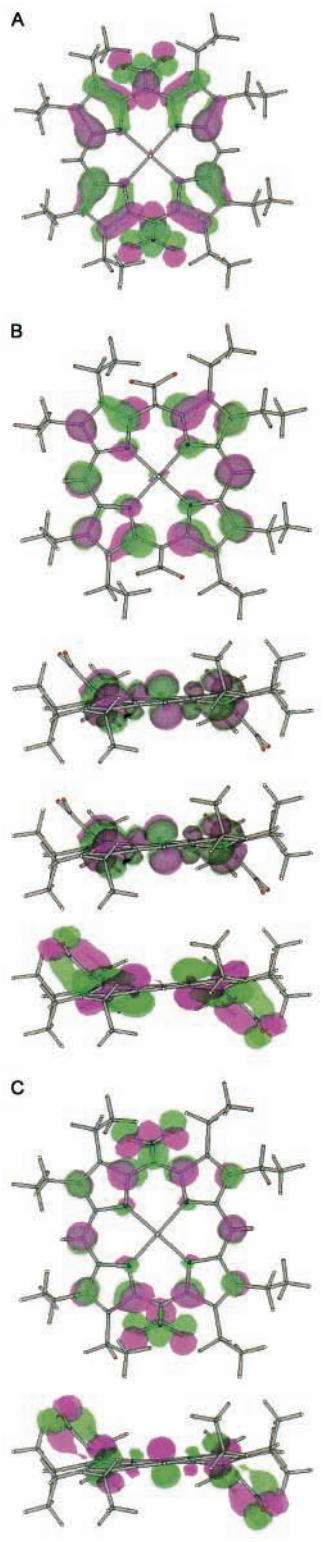

Figure 11. Horizontal and vertical views of three LUMOs of Ni(5,15-NO_2−OEP) as obtained from INDO calculations.

than that of the vertical conformers, notwithstanding the molecular mechanics calculations that predict the opposite, but it would contradict our Raman dispersion data, which are indicative of a very strong electronic interaction between the macrocycle and the NO_2 substituents. Different parameters for the N−O equilibrium bond distance and $-NO_2$ torsion parameters do not change this prediction, so this issue remains unresolved at present.

Summary

The present study shows that nitro substituents attached to the meso position have a significant impact on the electronic and structural properties of metalloporphyrins. They interact with the macrocycle by electron withdrawing and by $\pi\pi$ interactions. The latter give rise to an admixture of NO_2 orbitals into the ground and excited states of the macrocycle, which causes a break down of Gouterman's four-orbital model. This interaction also destabilizes the macrocycle and, thus, facilitates in-plane and out-of plane distortions. For Ni(5,15-diNO_2)OEP and Ni(5-NO_2−OEP) in CS_2, we obtained (at least) three different coexisting conformers with different ethyl orientations. They are all subject to strong ruffling, significant doming, and in-plane rhombic distortions along the methine bridges. Small saddling distortions are also present. The detected conformers most likely differ in terms of their saddling and doming distortions but show similar ruffling and rhombic distortions. The calculations predict that the nitro substituents are oriented horizontally, which facilitates their $\pi\pi$ interaction with the macrocycle. Conformers with vertical NO_2 orientations are higher in energy, and their population at room temperature is negligibly small. Comparison of the mono- and dinitro-substituted porphyrins reveals larger distortions for the latter. With respect to the in-plane rhombic distortion the influence of the nitro groups is nearly additive. Concerning their perturbative capacity, the NO_2 competes with very sterically demanding alkyl substituents such as *tert*-butyl.

Several yet unanswered questions arise from the results of this study. First, it is unclear how the energy diagram of the π-electron system is changed as a consequence of the break down of the four-orbital model. The absorption spectra look surprisingly normal, but we have experimental evidence for dramatic changes at cryogenic temperatures, which are still not understood (Lemke, Cupane, Leone, Schweitzer-Stenner, unpublished results). Optical absorption measurements by Hobbs et al.[25] have identified an absorption band which shifts from 347 nm in Ni(5-NO_2−OEP) to higher wavelengths with increasing nitro substitution. It may be assignable to a transition from the ground state to the highest of the three new, nondegenerate excited states formed by the interaction between the e_g orbitals and NO_2. Second, it is worth exploring the electronic structure of the excited states of 5,15-NO_2−porphyrins. The split Q and B states should always have one component that is electron-deficient in the macrocycle due to the delocalization over the NO_2 orbitals and another that is unperturbed. Hence, the former may serve as electron acceptor and the latter as donor in porphyrin chains.[38] The energy difference between these excited states can be modified by imposing additional B_{1g}-type distortions (rhombic distortions along the N−Me−N lines) using specific asymmetric substitution of the β carbons or by choosing a free-base porphyrin. Third, it would be of interest to learn about the influence of (asymmetric) nitro substitution on photoexcited d states of the metal, which because of the variability of their lifetime, have attracted considerable interest of researchers over the last 10 years.[39] Fourth, it may be of relevance for porphyrin design to compare the impact of meso- and β substituted nitro−porphyrins.

Acknowledgment. Part of this project was supported by the European Community in the Framework of the network program "The Dynamics of Protein Structure", which was part of the "Human Capital and Mobility Program". The experimental part of the work was carried out when C.L. was a graduate student in the laboratory of W.D. at the University of Bremen. The

theoretical analysis of the Raman data was finalized at the University of Puerto Rico. R.S.S. acknowledges support from the EPSCOR-NSF grant for "The Influence of Asymmetric and Non-Planar Distortions on Functional Properties of Metalloporphyrins in Solution and in Proteins" (PR EPSCOR Grant OSR-9452893). Sandia is a multiprogram laboratory operated by Sandia Corporation, a Lockheed Martin Company, for the United States Department of Energy under Contract DE-AC04-94AL85000.

Supporting Information Available: Relationships between the symmetries of porphyrin deformations and the Raman tensor of A_{1g}-, B_{1g}-, B_{2g}-, and A_{2g}-type modes; correlation tables for obtaining the vibronic perturbation symmetry of the second and third term in eq 6 for different symmetry types of porphyrin deformation. This information is available free of charge via the internet at: http://pubs.acs.org.

References and Notes

(1) Senge, M. In *The Porphyrin Handbook*; Kadish, K. M., Smith, K. M., Guilard, R., Eds.; Academic Press: San Diego, 2000; Vol. 1, p 239.
(2) Barkigia, K. M.; Chantranupong, L.; Smith, K. M.; Fajer, J. *J. Am. Chem. Soc.* **1988**, *110*, 7566.
(3) Scheidt, W. R.; Lee, Y. *Struct. Bonding (Berlin)* **1987**, *64*, 1.
(4) Plato, M.; Möbius, K.; Michel-Beyerle, M. E.; Bixon, M.; Jortner. J. *J. Am. Chem. Soc.* **1988**, *110*, 7279.
(5) Kadish, K. M.; Franzen, M. M.; Han, B. C.; Araullo-McAdams, C.; Sazou, D. *J. Am. Chem. Soc.* **1991**, *113*, 512.
(6) Shelnutt, J. A.; Song, X. Z.; Ma, J.-G.; Jia, S. L.; Jentzen, W.; Medforth, C. J. *Chem. Soc. Rev.* **1998**, *27*, 31.
(7) Franco, R.; Ma, J.-G.; Lu, Y.; Ferreira, G. C.; Shelnutt, J. A. *Biochemistry* **2000**, *39*, 2517.
(8) Song, X.; Miura, M.; Xu, X.; Taylor, K. K.; Majumder, S. A.; Hobbs, J. D.; Cesarano, J.; Shelnutt, J. A. *Langmuir* **1996**, *12*, 2019.
(9) Genteman, S.; Nelson, N. Y.; Jaquinod, L.; Nurco, D. J.; Leung, S. H.; Medforth, C. J.; Smith, K. M.; Fajer, J.; Holten, D. *J. Phys. Chem. B* **1997**, *101*, 1247.
(10) Jentzen, W.; Song, X.; Shelnutt, J. A. *Biophys. J.* **1998**, *74*, 753.
(11) Ravikanth, M.; Chandrashekar, T. K. *Struct. Bonding (Berlin)* **1995**, *82*, 105.
(12) Shelnutt, J. A. In *The Porphyrin Handbook*; Kadish, K. M., Smith, K. M., Guilard, R., Eds.; Academic Press: San Diego, 2000; Vol. 7, p 167.
(13) Ma, J.-G.; Zhang, J.; Franco, R.; Jia, S.-L.; Moura, I.; Moura, J. J. G.; Kroneck, P. M. H.; Shelnutt, J. A. *Biochemistry* **1998**, *37*, 12431.
(14) Song, X.-Z.; Jentzen, W.; Jia, S.-L.; Jaquinod, L.; Nurco, D. J.; Medforth, C. J.; Smith, K. M.; Shelnutt, J. A. *J. Am. Chem. Soc.* **1996**, *118*, 12975.
(15) Jentzen, W.; Song, X.-Z.; Shelnutt, J. A. *J. Phys. Chem. B* **1997**, *101*, 1684.
(16) Senge, M. O.; Medforth, C. J.; Forsyth, T. P.; Lee, D. A.; Olmstead, M. M.; Jentzen, W.; Pandey, R. K.; Shelnutt, J. A.; Smith, K. M. *Inorg. Chem.* **1997**, *36*, 1149.
(17) Schweitzer-Stenner, R. *J. Porphyrins Phthalocyanines* **2001**, *5*, 198.
(18) Zgierski, M. Z.; Pawlikowski, M. *Chem. Phys.* **1982**, *65*, 335.
(19) Schweitzer-Stenner, R *Q. Rev. Biophys.* **1989**, *22*, 381.
(20) Lemke, C.; Dreybrodt, W.; Shelnutt, J. A.; Quirke, J. M. E.; Schweitzer-Stenner, R. *J. Raman Spectrosc.* **1998**, *29*, 945.
(21) Lemke, C.; Schweitzer-Stenner, R.; Shelnutt, J. A.; Quirke, J. M. E.; Dreybrodt, W. *J. Phys. Chem. A* **2001**, *105*, 6668.
(22) Schweitzer-Stenner, R.; Stichternath, A.; Jentzen, W.; Song, X.-Z.; Shelnutt, J. A.; Faurskov Nielsen, O.; Medforth, C. J.; Smith, K. M. *J. Chem. Phys.* **1997**, *107*, 1794.
(23) Gouterman, M. *J. Chem. Phys.* **1959**, *30*, 1139.
(24) Unger, E.; Bobinger, U.; Dreybrodt, W.; Schweitzer-Stenner, R. *J. Phys. Chem.* **1993**, *97*, 9956.
(25) Hobbs, J. D.; Majumder, S. A.; Luno, L.; Sickelsmith, G. A.; Quirke, J. M. E.; Medforth, C. J.; Smith, K. M.; Shelnutt, J. A. *J. Am. Chem. Soc.* **1004**, *116*, 3261.
(26) Schweitzer-Stenner, R.; Bobinger, U.; Dreybrodt, W. *J. Raman Spectrosc.* **1991**, *22*, 65.
(27) Schweitzer-Stenner, R.; Dreybrodt, W. *J. Raman Spectrosc.* **1992**, *23*, 539.
(28) Schweitzer-Stenner, R.; Cupane, A.; Leone, M.; Lemke, C.; Schott, J.; Dreybrodt, W. *J. Phys. Chem.* **2000**, *104*, 4254.
(29) Shelnutt, J. A.; Medforth, C. J.; Berber, M. D.; Barkigia, K. M.,; Smith, K. M. *J. Am. Chem. Soc.* **1991**, *113*, 4077.
(30) Barkigia, K. M.; Renner, M. W.; Furenlid, L. R.; Medforth, C. J.; Smith, K. M.; Fajer, J. *J. Am. Chem. Soc.* **1993**, *115*, 3627.
(31) Stichternath, A.; Schweitzer-Stenner, R.; Dreybrodt, W.; Mak, R. S. W.; Li, X.-Y.; Sparks, L. D.; Shelnutt, J. A.; Medforth, C. J.; Smith, K. M. *J. Phys. Chem.* **1993**, *97*, 1993.
(32) Li, X. Y.; Czernuszewicz, R.; Kincaid, J. R.; Spiro, T. G. *J. Am. Chem. Soc.* **1989**, *111*, 7012.
(33) Lemke, C. Ph.D. Thesis, Universität Bremen, Bremen, Germany, 1997.
(34) Jentzen, W.; Unger, E.; Song, X.-Z.; Jia, S.-L.; Turowska-Tyrk, I.; Schweitzer-Stenner, R.; Dreybrodt, W.; Scheidt, W. R.; Shelnutt, J. A. *J. Phys. Chem. A* **1997**, *101*, 5789.
(35) Rush, T. S.; Kozlowski, P. M.; Piffat, C. A.; Kumble, R.; Zgierski, M.; Spiro, T. G. *J. Phys. Chem. B* **2000**, *104*, 5020.
(36) Senge, M. O.; Medforth, C. J.; Forsyth, T. P.; Lee, D. A.; Olmstead, M. M.; Jentzen, W.; Pandey, R. K.; Shelnutt, J. A.; Smith, K. M. *Inorg. Chem.* **1997**, *36*, 1149−1163
(37) Laycock, J. D.; Ferguson, J. A.; Yost, R. A.; Quirke, J. M. E.; Rohrer, A.; Ocampo, R.; Callot, H. *J. Mass. Spectrom.* **1997**, 978−983.
(38) Tsuchiya, S. *J. Am. Chem. Soc.* **1999**, *121*, 48−53.
(39) Drain, C. M.; Gentemann, S.; Roberts, J. A.; Nelson, N. Y.; Medforth, C. J.; Jia, S.; Simpson, M. C.; Smith, K. M.; Fajer, J.; Shelnutt, J. A.; Holten, D. *J. Am. Chem. Soc.* **1988**, *110*, 3781.